Engineering Failure Analysis 118 (2020) 104789

Contents lists available at ScienceDirect

Engineering Failure Analysis

journal homepage: www.elsevier.com/locate/engfailanal

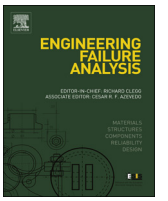

Probabilistic modelling of the robustness of reinforced concrete frames accounting for material property variability using a layered beam finite element approach

Batoma Sosso[a], Sarah da Silva Andrade[b], Luiz C.M. Vieira Jr.[b], Péter Z. Berke[a,*]

[a] Building, Architecture and Town Planning (BATir) Department, CP 194/2, Université libre de Bruxelles (ULB), Av. F.D. Roosevelt 50, 1050 Brussels, Belgium

[b] Departamento de Estruturas (FEC), Universidade Estadual de Campinas, Av. Albert Einstein, 951, CEP: 13083-852, Campinas SP, Brazil

ARTICLE INFO

Keywords:
Finite element analysis
Structural failures
Probability
Correlations
Mechanical properties
Failure mechanism

ABSTRACT

In this contribution the influence of material properties variability on the structural robustness of Reinforced Concrete (RC) frames is assessed using a computational approach. A layered beam finite element model is employed in a correlation reduced Latin Hypercube Sampling-based stochastic framework in which the material parameters driving the elastic, plastic and fracture behavior of both steel and concrete constituents are considered to be Random Variables (RVs). The probability characteristics of each RV are set to match relevant experimental data available in the literature. Structural robustness of each deterministic simulation is evaluated based on the outcome of a nonlinear dynamic progressive collapse computation using the Sudden Column Loss (SCL) scenario. The sensitivity of structural robustness and residual displacement to each material parameter is established first, considering their variations separately. The robustness of a RC frame designed following the European building code, incorporating all RVs simultaneously is assessed and critically compared to the results of the sensitivity analysis. The link between the structural degradation and failure mechanism and data extracted from the cross sectional behavior is established. The identification of structural mechanisms inducing failure or survival is attempted and a set of practically relevant recommendations for progressive collapse resistance is listed.

1. Introduction

Ensuring structural robustness is a key requirement in structural design and is prescribed in building codes [1–4]. It is natural that during the building design and construction process there are numerous sources of uncertainties [5] and therefore, ensuring structural robustness is critically dependent on the random nature of the material properties of the constituents, loads, construction and cross sectional geometries [5,6]. This is usually taken into account by safety factors in the design standards, aiming for ensuring reliability and robustness of structures with a low computational cost, in a simplified approach. It has been recognized that a more thorough assessment of the influence of the material and design parameters variability is of interest [7–10,6,11], allowing for a more in-depth understanding of the underlying complex phenomena and interaction between these variables of intrinsically random nature.

There are several works devoted to steel frames considering uncertainty in material properties and live load [7], geometrical

* Corresponding author.
E-mail address: pberke@ulb.ac.be (P.Z. Berke).

https://doi.org/10.1016/j.engfailanal.2020.104789
Received 13 November 2019; Received in revised form 16 July 2020; Accepted 4 August 2020
Available online 11 August 2020
1350-6307/

imperfections [12], steel connection behavior [9] and the sensitivity of the progressive collapse (PC) mechanism to uncertain design parameters [8]. This work gives a contribution to *the investigation of the probabilistic behavior in reinforced concrete (RC) structures against PC* which is a topic of increasing interest in the recent years. Even though, adding concrete in the structure naturally enhances its random nature considering the large variability of concrete's material parameters, the relatively moderate number of contributions/studies is probably due to the fact that RC structures can become complex to model and computationally more expensive than pure steel frames. RC is a heterogeneous composite and both constituents have very different mechanical behavior. In addition, the random characteristics of each material lack a common database agreed upon, there are various models available in the literature. Because of these limitations, most of the numerical work was devoted to deterministic PC analysis [13–18] where one or more columns were removed suddenly in a RC structure.

To assess the probabilistic behavior of RC structures Le and Xue [10] developed a two-scale stochastic finite element. A set of coarse-scale cohesive elements were used to represent the potential damage zones, such as beams, columns and joint panels. Latin Hypercube Sampling (LHS) technique was used to perform stochastic simulations of 2D RC frames under Sudden Column Loss (SCL) scenario, with uncertainties in both material properties and dead loads. It was shown that the model could successfully capture various collapse mechanisms of RC frames but the main bottleneck of this model is the calibration of the cohesive elements parameters. Brunesi et al. [19] developed a fiber-based model and performed Incremental Dynamic Analysis (IDA) where random variables (RVs) were generated by Monte Carlo Simulations (MCS). The approach was used to investigate two low-rise RC building classes: regular design (i.e. Eurocodes 2 [1]) and an earthquake resistant design (i.e. Eurocodes 8 [20]) considering 2D and 3D models, incorporating uncertainties related to the geometry of the structural members, the material properties and dead loads. They proposed fragility functions at multiple damage states and showed the influence of both building classes and 2D vs 3D models. Xiao et al. [6] conducted uncertainty and sensitivity analysis to demonstrate the influence and significance of randomness in PC analysis. The randomness of dead loads, material properties, and construction geometries (i.e. column height, beam length, etc.) on the performance of RC frame structures subjected to ground column loss were taken into account. A correlation-reduced LHS method was used to investigate the variability of RVs on the response of RC frames, showing that uncertainties have significant effects on the behavior of RC frames to mitigate PC. One of the recent works is the study of Feng et al. [11] who employed the Probability Density Evolution Method (PDEM) to perform static push-down analysis of two benchmark column removal tests using fiber beam finite elements. The authors investigated the influence of material properties and uncertain geometrical parameters on the global and local behavior of RC sub-assemblages. However, this work is limited to a relatively small frame, neglecting force redistribution that may spread beyond the elements connected to the removed column [16,15].

Recently, [21] used a probabilistic approach to investigate the influence of modelling strategies on the uncertainty propagation and on the ultimate load-bearing capacity of RC slabs. A global variance-based sensitivity analysis [10] was used, in which material and geometrical uncertainties were incorporated. It has been observed that the choice of modelling approaches i.e. analytical (e.g. rigid-perfectly plastic) or numerical (e.g. plastic hinge, fiber model) has a significant influence on the estimated probability of failure for a given structural system.

The vast majority of the numerical approaches above use commercial software [10,22] or open source software, such as OpenSees [23] or SeismoStruct [24] with a limited set of constitutive models by default [6,11]. In this contribution a computational approach based on probabilistic sampling to assess the structural robustness of a RC frame designed following the Eurocode [1] is proposed using an in-house developed framework with full control of the numerical ingredients and considering a large frame and SCL scenario. As opposed to a single, deterministic, simplified simulation using safety factors [13–16,18,17,25], a number of RVs are directly incorporated in the thousands of computations of this work using appropriate sampling methods [6,26,27].

Various sets of Random Variables are considered in the literature going from material [28,10,11,19,6], to load [29,19] and geometrical [19,6,21,11] parameters. As expected, when a large number of RVs are incorporated in the computational model, the required number of nonlinear computations skyrockets with a prohibitive computational cost, especially for realistic, large structures. Therefore it is essential to reduce the RVs to the smallest, most relevant set in a stochastic approach using complex nonlinear FE simulations. From the literature, the material properties were prone to exhibit the largest dispersion [28,10,11,19,6], especially in the case of concrete, when compared to cross sectional geometries for instance. Consequently, deterministic cross sectional geometries (e.g. width, height, reinforcement area) are assumed in this work, focusing rather on the variability of the material properties. In previous studies [6,21,11] material properties such as concrete and steel strengths have been shown to have a large influence in RC frames response. These are extended here with parameters governing the failure of concrete and steel, i.e. ultimate strain values are additional RVs with respect to the available literature, to the author's best knowledge. *The influence of concrete ductility on the PC response of RC frames is thereby investigated by considering unconfined and confined concrete cases using phenomenological constitutive models incorporating different ultimate strains*. Ultimate strain based conditions that govern layer fracture in the present model are not always incorporated in computational approaches. Our goals for considering frames also with low confinement, referred to as unconfined cases for the sake of brevity, with a physically sound stochastic ultimate strain include highlighting the importance of incorporating this parameter in a numerical model, as well as demonstrating and quantifying the effect of the ultimate strain range in which the structure can operate.

Noteworthy originalities of this work are the use of an in-house developed multilayered framework with full control of the numerical ingredients (i) to investigate the sensitivity of each RV on the PC behavior of a realistic large RC frame designed following Eurocode 2; (ii) the study of the influence of each RV on the residual deformation of frames that survive column loss; (iii) the critical assessment of the robustness of this frame when incorporating all RV simultaneously including the ultimate strains of both constituents; (iv) the exploitation of the layered beam approach to establish a link between the cross sectional behavior and the structural failure or resistance to progressive collapse and the identification of survival and failure modes of the structure.

This contribution is structured as follows. Section 2 presents briefly the main concepts of the computational tool based on a corotational layered beam model incorporating elasto-plastic material behavior and layer fracture for concrete and steel, together with the correlation reduced LHS random sampling method used in this work. Section 3 presents the numerical models for the RC frame and Section 4 the sensitivity study of each RV separately. Section 5 is dedicated to the assessment of the robustness of the frame considering all RVs simultaneously and linking the findings to the sensitivity study. In this section a link is built between the cross sectional behavior and the structural failure or resistance to progressive collapse. In Section 6 the main conclusions are highlighted, a set of practical recommendations are suggested to mitigate PC in RC frames and future research is proposed.

2. Computational modelling

2.1. Corotational layered beam model

Several computational modelling efforts for RC structures consider layered beam formulations [16,18,30,31]. It is a popular, accurate, but costly numerical technique, available today in open source codes as well [24,23], though with a restricted range of material models by default. The computational tool used in the present work is based on a multilayered beam approach [16], coupled with geometrically nonlinear kinematics [18]. The framework is based on a co-rotational Bernoulli beam formulation, where rigid body rotation is decoupled from strains by defining a local system of axes rotating with the beam [32]. This modelling strategy allows deriving physically motivated relationships between generalized stresses and strains at the sectional level and a gradual sectional strength degradation can be captured as a consequence of the progressive failure of the layers based on an ultimate strain criterion. In the current model the effects of stirrups are represented phenomenologically by increasing the ultimate strain of confined concrete defining different ranges of the ultimate strain of concrete corresponding to the highly confined regime (mean ultimate strain of 0.8%) and the regime with low confinement, referred to as the unconfined cases (mean ultimate strain of 0.35%). In reality, the presence of stirrups results in the confined concrete core in: (i) a somewhat higher yield strength of concrete due to the multi-axial stress state and more importantly (ii) a significantly larger ultimate strain of concrete, i.e. the ductility of concrete is increased [17,33–36]. Although other, physically sound approaches exist for stirrups consideration (see [30] and references within), they are not used here because of the large additional computational cost it induces to consider additional equilibrium equations on the cross sectional level. This simplification also implies that stirrups fracture is not accounted for as a possible failure mode. The multilayered beam model and resulting multi scale computational scheme are sketched in Fig. 1. The cross-section of structural members is discretized into a finite number of longitudinal layers (at least 60 layers for columns and 80 for beams) in which one-dimensional elasto-plastic constitutive equations for concrete and steel are applied. The cross sectional behavior of the finite element is thus directly derived by integration of the stress–strain response of the layers. The total axial strain in each layer ($\varepsilon^i_{x,tot}$) is computed from

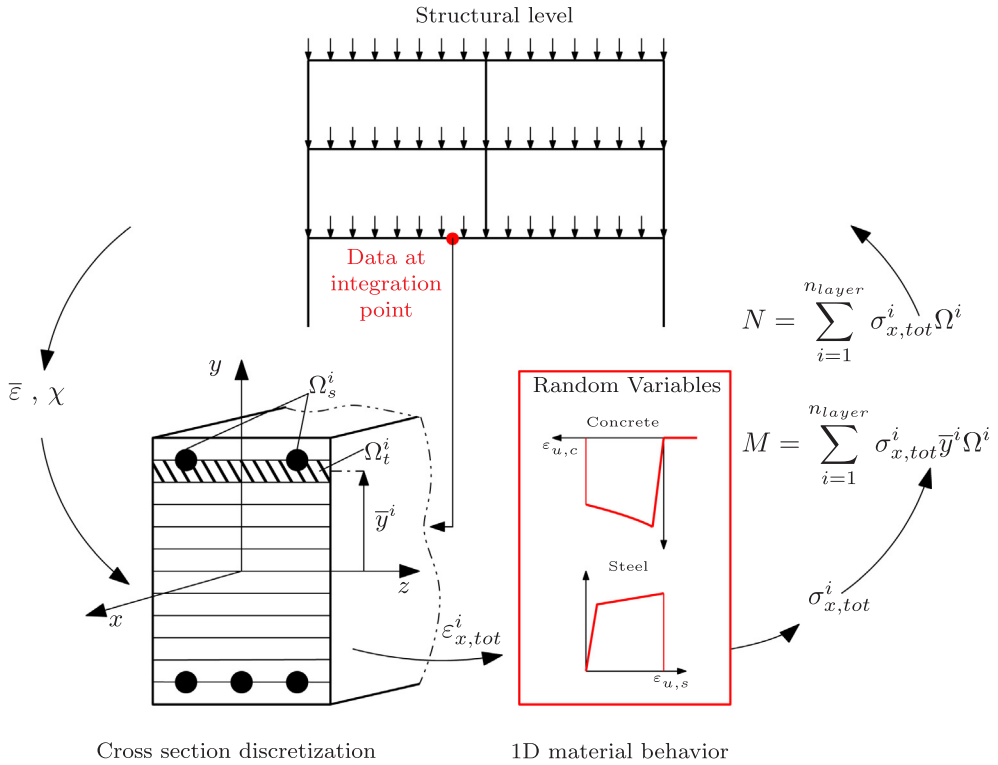

Fig. 1. Multilayered beam model and resulting multi scale computational scheme.

the generalized beam strains following Bernoulli kinematics (Eq. (1)).

$$\varepsilon^{i}_{x,tot} = \bar{\varepsilon} - \bar{y}^{i}\chi \tag{1}$$

where $\bar{y}^{i}$ is the average vertical coordinate of layer i computed from the sectional center of gravity, $\bar{\varepsilon}$ is the mean axial strain of the beam and χ, is curvature. Perfect bonding between concrete and steel is assumed, leading to strain compatibility (i.e. $\varepsilon^{ci}_{x} = \varepsilon^{si}_{x} = \varepsilon^{i}_{x,tot}$), where ε^{ci}_{x} and ε^{si}_{x} are the axial strain in concrete and steel at a given layer i, respectively. While the total strain is the same in a layer, the elastic and plastic strains are allowed to be different in the two constituents, as well as the stress that is generated in each material (following hardening for steel and softening for concrete). It is noteworthy, that the introduction of bond slip representation in the layered beam formulation, as in [37], would allow incorporating a failure mechanism that is currently unaccounted for. In the present contribution this was not attempted to keep the computational effort reasonable for the large number of simulations performed in this stochastic analysis incorporating essential features, such as elasto-plastic material behavior and layer fracture.

The stress in both materials is computed independently. The composite layer's axial stress ($\sigma^{i}_{x,tot}$) is obtained using a weighted stress average based on the steel volume fraction in a layer by the following expression:

$$\sigma^{i}_{x,tot} = \frac{\Omega^{i}_{t} - \Omega^{i}_{s}}{\Omega^{i}_{t}}\sigma^{ci}_{x} + \frac{\Omega^{i}_{s}}{\Omega^{i}_{t}}\sigma^{si}_{x} \tag{2}$$

where Ω^{i}_{t} and Ω^{i}_{s} are the total cross sectional area of a layer and the longitudinal reinforcement cross sectional area in the layer respectively. $\sigma^{ci}_{x}(\varepsilon^{ci}_{x})$and $\sigma^{si}_{x}(\varepsilon^{si}_{x})$ are the axial stress in concrete and steel, respectively. Having $\sigma^{i}_{x,tot}$ computed for all of the layers, the cross sectional generalized stresses (i.e. N = normal force and M = bending moment) are evaluated as a finite sum of the contributions of each layer (Fig. 1). It is noteworthy to point out that the whole history of bending moment vs. curvature data is available for each simulation naturally at each integration point of each finite element, that can be very useful for calibrating cheaper plastic hinge based numerical models.

The 1D constitutive law used for concrete is assumed with zero tensile strength, as in [30,18]. The concrete compressive elasto-plastic behavior [16] is described by Eq. (3).

$$\sigma^{c}_{x} = f_{c}\exp(\mu_{c}\kappa_{c}) \tag{3}$$

where σ^{c}_{x} is the current compressive yield stress, f_{c} the initial compressive yield stress, μ_{c} and κ_{c} are the softening parameter ($\mu_{c} \leqslant 0$), and the cumulated plastic strain in concrete, respectively.

The reinforcements are described using a 1D bilinear elasto-plastic model symmetric in traction and compression as in [16,18] given by the following expression:

$$\sigma^{s}_{x} = f_{y}(1 + \mu_{s}\kappa_{s}) \tag{4}$$

where σ^{s}_{x} is the current steel compressive/tensile yield stress, f_{y} is the initial yield stress, μ_{s} and κ_{s} are the hardening parameter and the cumulated plastic strain, respectively. The developed multilayered framework allows capturing the layer by layer failure of each material by comparing the total strain in a material to its ultimate strain (being an input material parameter). Stresses in a material are set to zero once its ultimate strain is reached. A cross sectional strength degradation as a consequence of the layer by layer failure, resulting in a sectional strain-softening behaviour is thus incorporated. The constitutive models resulting from these modelling assumptions are shown in Fig. 2.

In summary, four parameters govern the material behavior for each constituent: Young's modulus (E_{c}), compressive strength (f_{c}), softening parameter(μ_{c}), ultimate strain ($\varepsilon_{u,c}$) for concrete and Young's modulus (E_{s}), yield strength (f_{y}), hardening parameter (μ_{s}), ultimate strain $\varepsilon_{u,s}$ for reinforcement. Out of these six are taken as RVs in the subsequent simulations. Although deriving stochastic parameters directly from experimental data is an interesting approach, sufficient data for stochastic representativity of experimental tests for steel rebar behavior, confined concrete and unconfined concrete behavior of the used diameters and concrete grade, respectively, was not available. As a next best solution, in order to ensure practical relevancy of the computational results, our approach consisted in feeding each random parameter (elastic modulus, yield strength and ultimate strain) separately from dedicated data

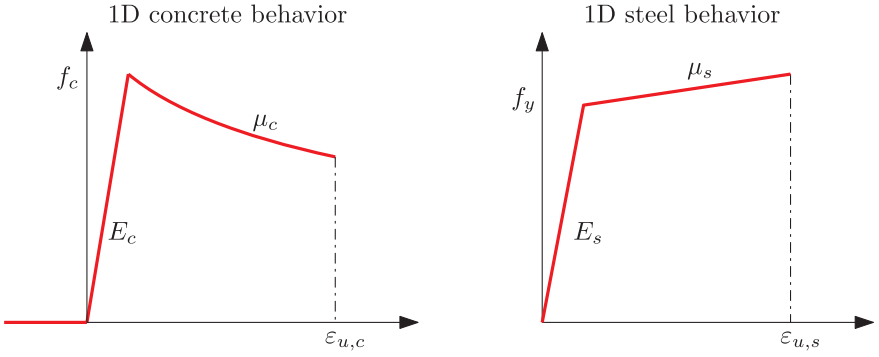

Fig. 2. 1D elasto-plastic constitutive behavior for concrete in compression (no tensile strength) and steel in traction/compression.

available in the literature [38–42]. Because of lack of statistical data, the parameters μ_c and μ_s are set to their deterministic values (i.e. $\mu_c = -5$[30] and $\mu_s = 1.5$[18]), as adopted in previous works [6,11,43]. It is important to point out that the softening and hardening parameters also exhibit a large dispersion in a real life data. Not incorporating them as RV can be explained by a sensitivity study of these parameters (±30% of nominal values) that showed a low sensitivity of the structural response of confined concrete frames that survived column loss. This implies that even though the hardening and softening in the plastic domain are not considered random, the material parameters governing the elastic behavior, the elasto-plastic transition and fracture are incorporated as RV; the latter two (i.e.$\varepsilon_{u,c}$ and $\varepsilon_{u,s}$) are key to capture the nonlinear structural response due to cross sectional degradation exhibited in PC simulations.

2.2. Random sampling method

The standard MCS method is a well-known technique in statistics but with an inherently high cost when a large number of RV are considered [19]. As numerical models become complex (e.g. nonlinear dynamic structural behavior), resulting in an increasing computational effort, alternative sampling methods are necessary. Latin Hypercube Sampling has been widely used to analyze structural collapse resistance probabilistically [6,29,43,10,44–46], because it can drastically reduce the number of simulations necessary to achieve reasonably accurate results. In this work, LHS with correlation reduction [27,26] is used to avoid any undesired correlation between variables, as suggested by [6].

2.2.1. Concrete properties as RV

Three concrete material parameters were selected as random variables. E_c and f_c are assumed to follow normal distributions with coefficients of variation (CoV) as recommended by Mirza et al. [38] and Ellingwood et al.[39], respectively. Two sets of $\varepsilon_{u,c}$ are defined to represent phenomenologically confined and unconfined concrete behavior. For unconfined concrete, $\varepsilon_{u,c}^{uc}$ is based on Trezos [40] whereas for confined concrete a uniform function of $\varepsilon_{u,c}^{c}$ between 0.7% and 0.9% is assumed. Considering a normal distribution for this parameter was observed to yield practically the same results, as explained in Section 4. The choice of the statistical model for $\varepsilon_{u,c}^{c}$ in the present simulations does not appear to be critical for the assumed range values. A correlation of 0.8 is considered among f_c and E_c, as adopted in [6] based on [47] recommendations. The other parameters are assumed to be independent variables (Table 1).

2.2.2. Steel properties as RV

The steel Young's modulus E_s is modeled according to Mirza and MacGregor [41] whereas f_y and $\varepsilon_{u,s}$ follow the Probabilistic Model Code (PMC) [42]. The dispersion of steel material parameters is much lower than of concrete, as expected. However, their variability is critical to the collapse response of the RC frame, especially at the Catenary Action (CA) stage as it will be shown in Section 4 and 5. Statistical distributions for steel parameters are summarized in Table 2. It is important to note that the nominal value of the ultimate strain of steel is 4%, as in [16], which corresponds to a ductility between classes A and B in Eurocode 2 [1] and a bias factor of 1.12 is assumed for f_y as defined in [42].

The Probability Density Function (PDF) of the RV are graphically presented in Fig. 3 for unconfined and confined concrete cases.

3. Structural computational model

To investigate the sensitivity of the structural response to the SCL scenario to uncertainties and their influence, a plane frame designed according to Eurocode 2 [1] is studied. The building from which it's extracted from is composed of 5-storeys and 8 bays [16,18], corresponding to a 48 m long and 18 m high office building. The 2D frame model of the structure is subject to the loss of the ground floor middle column. The insight offered by 2D models when proper design and detailing is considered has been duly recognised in the literature and several contributions remain limited to this scenario [48,44,10,14]. The employed finite element model has been shown to capture well the behavior of planar reinforced concrete frames, also in sudden column removal scenarios [16,18]. The inherent low computational cost of the 2D numerical model is crucial for the stochastic analysis based on a large number of simulations performed in this work. To reduce the computational cost, only half of the structure is modelled (Fig. 4). The frame was designed [16] based on Eurocode 2 [1] using the commercial software Diamonds by Buildsoft [49]. For the sake of simplicity, three different cross sections were considered: all of the columns have the same geometry from the ground to the top floor and two types of beams are used (hogging and sagging sections). The main reinforcements were assumed as continuous and the continuity of 2/3 of hogging reinforcements were considered in the designs, which according to the GSA [3] is vital for resisting the load reversals that

Table 1
Statistical distributions of concrete and uncertainty parameters.

Material	Parameter	Nominal	CoV	Distribution	Reference
Concrete	E_c	32 *GPa*	0.077	Normal	[38]
	f_c	37.9 *MPa*	0.18	Normal	[39]
	$\varepsilon_{u,c}^{uc}$	0.35%	0.143	Normal	[40]
	$\varepsilon_{u,c}^{c}$	0.8%	[0.7–0.9%]	Uniform	–

[uc] Unconfined concrete; [c] Confined concrete

Table 2
Statistical distributions of steel random variables and uncertainty parameters.

Material	Parameter	Nominal	CoV	Distribution	Reference
Steel	E_s	200 GPa	0.033	Normal	[41]
	f_y	500 MPa	0.054	Normal	[42]
	$\varepsilon_{u,s}$	4 %	0.09	Normal	[42]

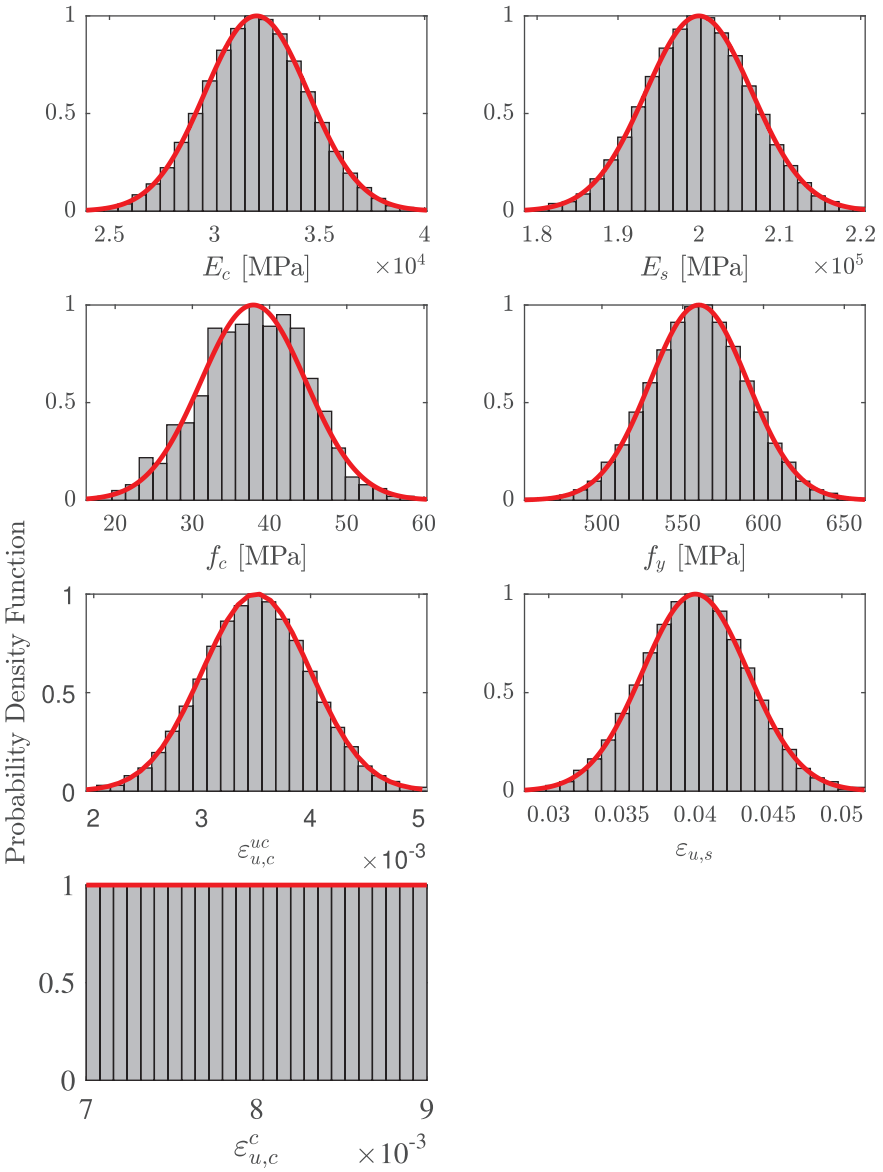

Fig. 3. Normalized Probability Density Function of the RV incorporated in the PC simulations.

follow the loss of a primary support. Stirrups are given in the design and they can be represented in the numerical model phenomenologically by increasing the ultimate strain of concrete (but neglecting the relatively lower relative strength increase).

A concrete cover of 50 mm was assumed. The vertical load combinations to be applied on the structure are those suggested by DoD [2] given in Table 3 and the main reinforcement details are shown in Fig. 5.

Nonlinear dynamic analysis are performed by using an implicit Newmark scheme, as in [16,18]. A numerical damping of 5% as in [19,50,28,51,18,16] is adopted to reduce the irrelevant high frequency vibrations in the structural response. This 5% damping refers to the Newmark time integration scheme parameters and structural damping by plastic dissipation is incorporated naturally in the

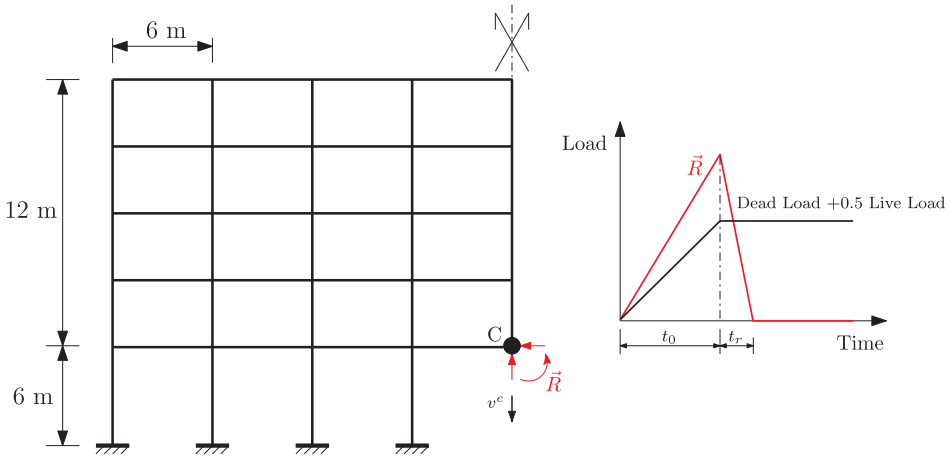

Fig. 4. Half of the five-storey frame considered in this study due to the symmetry of the structure and loads and boundary conditions [16].

Table 3
Loads applied to the structures.

	Floor			Roof		
	Dead	Live	Total	Dead	Live	Total
Loads (kN/m)	43.2	18	52.2	43.2	6.0	46.2

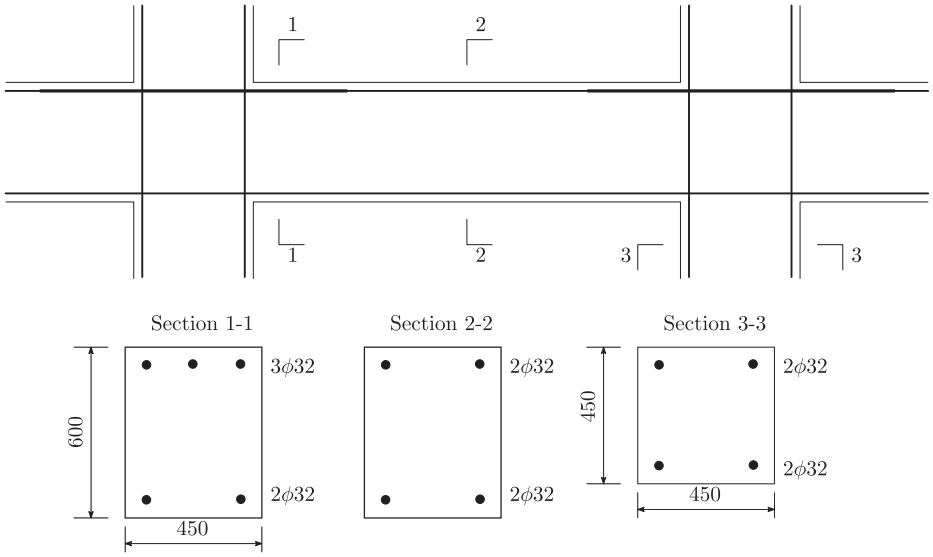

Fig. 5. Cross sectional reinforcement details (dimensions in mm).

layered beam formulation through the elasto-plastic behavior of the constituents in the layers. The SCL [16,18,15] scenario is employed, because it provides a reasonable balance between the usefulness of the results and the cost of the simulation effort to be paid [52]. In the simulations, the reaction forces at the top of the column to be removed (point C in Fig. 4), $\vec{R}_C = [F_x;F_y;M_z]$, are incremented together with the live and dead loads during $t_0 = 100$ s to avoid unwanted dynamic effects. The SCL analysis starts by removing suddenly these reaction forces while maintaining all other loads constant (Fig. 4). The removal time t_r is set to 10 ms to simulate an instantaneous column loss, as recommended in [16,18]. The dynamic analysis time span after column removal is taken as 2 s. It was observed that in 2 s the conclusion can be drawn whether the structure collapses or withstands the loss of the column [14,16,18]. Structural robustness is assessed based on the vertical displacement of the node C vs. time data, as well as on the state of the cross sections (e.g. reinforcement failure detection). The finite element length is taken approximatively equal to the cross sectional height in order to ensure proper energy dissipation with a softening behavior, i.e. in a volume close to the plastic hinge volume [16]. Each frame is discretized into 408 finite elements with 1179 degrees of freedom (DOF). An average of 90 minutes is required to

perform a single dynamic simulation, on a High Performance Computing (HPC) cluster where simulations were run in parallel, each using a single thread on Intel Skylake -Xeon Gold 6126 with CPU 32 GB of memory. By running over 100 simulations at the same time 1000 simulations took approximatively 12 h when the cluster was free from other jobs and up to a day when the cluster resources were shared intensively. In this work the results of a total of more than 12.000 simulations are discussed, corresponding to approximately one week of computations on a HPC cluster.

4. Sensitivity study

The aim of this sensitivity analysis is to investigate the influence of the variability of each material parameter separately on the structural behavior, to classify them as function of their criticality and to assess how such uncertain parameters affect a realistic RC frame's performance to resist PC. In the subsequent simulations all but one material parameters are fixed to their nominal (i.e. reference) values, while a single chosen parameter is varied.

4.1. Sensitivity analysis methodology

In the following methodology, structures will be referred as survived (i.e not collapsed) if the vertical displacement of the node C in Fig. 4 is asymptotically limited in the time frame of the dynamic analysis (i.e. 2 s after column loss). On the other hand a frame is recognized as collapsed if it has a monotonously increasing vertical displacement that reaches -0.5 m, set as a limit at which the simulation automatically stops.

Similar to [21], when the number of samples is sufficient (i.e. converged), the progressive collapse resistance of the system can be estimated by the probability of failure (p_f); as defined in Eq. (5).

$$p_f = \frac{n_c}{N_{tot}} \tag{5}$$

with n_c the number of collapsed frames and N_{tot} the total number of samples. The purpose of p_f here is simply to identify the most critical RV for the collapse of the structure rather than actually accurately quantifying the probability of failure. In order to analyze the influence and importance of the number of samples in the simulations, a convergence analysis was carried out for the unconfined concrete case incorporating all RVs with 100, 1000, 5000 and 10000 simulations. The probability of failure already converged at 1000 simulations. The choice was made that all further analyses are also performed with 1000 correlation reduced LHS samples (i.e. $N_{sample} = 1000$).

Note that for the confined concrete cases the probability of failure is significantly lower because of the higher concrete ultimate strain, as it will be shown in Section 4.2. It is assumed here that the number of samples determined as sufficient for unconfined concrete case also yield qualitatively representative results for the confined concrete case. It has to be emphasized that increasing the number of samples substantially could result in an unaffordable computational cost and quantifying p_f accurately is not the objective here.

Furthermore, to investigate the RV influence on the residual deformation of survived frames, the maximum (v^c_{max}) and minimum (v^c_{min}) values of the monitored vertical displacement of point C after column loss were computed for each set of simulations. This residual vertical displacement variation is an indicator of the sensitivity of the structure to irreversible events after column loss and will be discussed in details in the Section 4.2.2.

4.2. Results of the sensitivity analysis

The vertical displacement time-histories of point C for each RV are plotted in Figs. 6 and 7 for unconfined and confined concrete cases, respectively. The first observation is that with the reference material parameter set for unconfined concrete (i.e. nominal values), the frame collapsed while it survived in the confined concrete reference case. The most striking result is that because of material properties variability with realistic stochastic parameters for each RV, some frames collapsed while others survived. The second main finding is that frames in the unconfined concrete case are significantly more prone to collapse after column loss than frames using the confined concrete model with higher concrete ultimate strain. The ultimate strain of concrete ($\varepsilon_{u,c}$) is thus a key parameter for PC mitigation of RC frames and concrete ductility is critical to ensure by appropriate stirrups in the design.

Regarding the collapse time for unconfined concrete, the RVs $\varepsilon^{uc}_{u,c}$, E_c, f_c, and f_y show the largest dispersion. This is mainly due on the one hand to the large variability of f_c and $\varepsilon^{uc}_{u,c}$ (see Table 1) and on the other hand to the influence of the steel yield strength f_y to delay or advance reinforcement yielding.

Additionally, in both concrete cases, for high values of the reinforcement yield strength, the structural response for survived frames is oscillatory after column loss with large amplitudes. This is explained by the fact that high values of f_y, leads to a more elastic structural response promoting the exchange of stored strain and kinetic energy. Conversely, low values of f_y, induce earlier reinforcement yielding and a high plastic energy dissipation resulting in lower amplitude oscillations, as shown in Figs. 6 and 7.

The variation of material parameters E_s and $\varepsilon_{u,s}$ for unconfined concrete led to the collapse for all of the 1000 simulations in the set. The identical failure mode was observed for these RVs, characterized by reinforcement yielding followed by concrete crushing (in less or more than 30% of the cross sectional area for the earliest and latest collapsed frames, respectively) closely followed by reinforcement fracture, as in the reference case. This finale failure explains the observed dispersion in collapse time as function of $\varepsilon_{u,s}$. E_s was observed to have a limited influence in both unconfined and confined concrete cases. The variation of this RV never led to

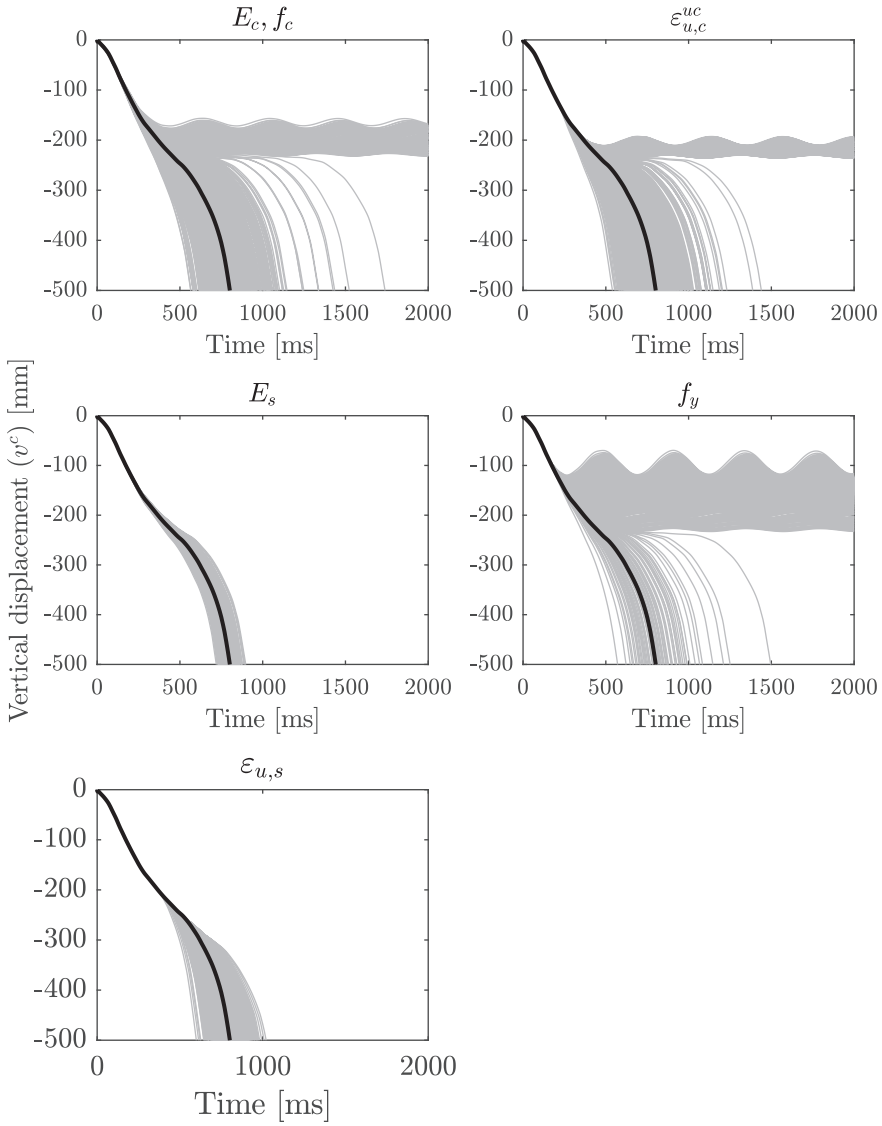

Fig. 6. Vertical displacement of point C (v^c) vs time histories for the unconfined concrete cases. The solid black curve corresponds to the simulation with the nominal material parameter set for unconfined concrete and each figure shows the results of 1000 simulations.

switching between structural survival or collapse states (as opposed to E_c, f_c for example). This can be explained by the fact that the elastic modulus of steel mainly influences the structural responses in reversible regime, while SCL induces primarily an irreversible response.

It is noteworthy that varying $\varepsilon_{u,c}^{c}$ and $\varepsilon_{u,s}$ yielded practically the same displacement–time curves for survived confined concrete frames. This statement is limited only to these survival cases, it is not a generic conclusion. Both ultimate strain variables are of utmost importance in the structural response, however in the confined concrete case not leading to structural failure their influence within their assumed range (fitted to experimental data, when possible) was observed to be limited on the displacement vs. time data. This is not true for the other cases considered in this contribution. As depicted in Fig. 9, beyond 0.41% ultimate strain of concrete (i.e. keeping the rest of RVs at their nominal values), the frame survives SCL. This explain why the structural response is insensitive to variations of $\varepsilon_{u,c}^{c}$ in the confined concrete case; the values of ultimate strain of concrete are higher than 0.5% (see Fig. 3).

Analysing the vertical displacement curves together with the cross sectional data at relevant parts of the structure, survival structural mechanisms can be identified. The damage mechanism leading to the survival for the unconfined concrete cases was identified to be: (i) the tensile yielding of the reinforcement, succeeded by (ii) concrete crushing (± 30% of the cross sectional area) and (iii) eventually axial layer strains close to the ultimate strain of steel, without inducing tensile reinforcement fracture. The majority of survived frames in the confined concrete case undergo only the tensile yielding of the reinforcement, except for the largest residual vertical displacement for E_c, f_c. This last case experienced the progressive yielding of the reinforcements with low intensity concrete crushing (in less than 30% of the cross sectional area) followed by the gradual bottom to top floor tensile rebars fracture

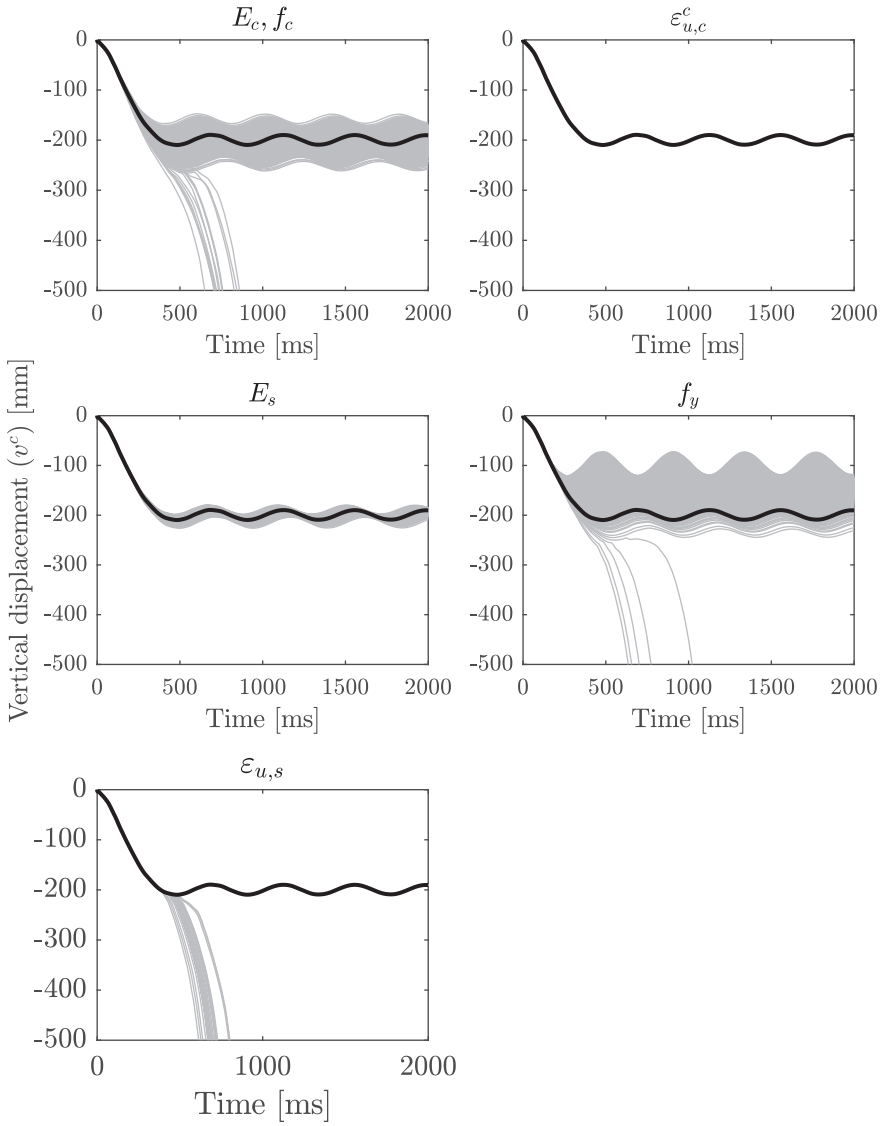

Fig. 7. Vertical displacement of point C (v^c) vs time histories for the confined concrete cases. The solid black curve corresponds to the simulation with the nominal material parameter set for confined concrete and each figure shows the results of 1000 simulations.

except the roof floor which undergo only the yielding of tensile reinforcement.

4.2.1. Probability of failure assessment

The probability of failure p_f is reported in Fig. 8. For unconfined concrete, results show that the concrete ultimate strain $\varepsilon^{uc}_{u,c}$ and correlated RV E_c, f_c have the largest influence. Fig. 9 shows that the majority of the sample for $\varepsilon^{uc}_{u,c}$ and E_c, f_c are in the unsafe domain, i.e. leading to collapse. Their relatively low nominal values and their critical role in the chain of the survival mechanism governing concrete yielding and crushing explains the high probability of failure of 86.9% and 81.7%, respectively for $\varepsilon^{uc}_{u,c}$ and E_c, f_c. The 100% p_f in Fig. 8 can be explained by the reference case with the nominal material parameter set collapsing, being the case around which the RVs are varied. The impact of varying E_s and $\varepsilon_{u,s}$ is limited, not leading to cases of survival in the unconfined concrete case.

The yield strength of steel f_y presents a lowest probability of failure of 5.9%, first because of the bias factor of 1.12 adopted for f_y. The bias factor relates the mean value obtained from the experimental test with the nominal value to take into account the deviations in structural conditions and the ones testing [42].

The results from probability of failure assessment show a clear cut separation between confined (low p_f) and unconfined concrete cases (higher p_f) with a much lower probability of failure for $\varepsilon^c_{u,c}$. This conclusion was verified to hold for a normal distribution model for $\varepsilon^c_{u,c}$ as well (with CoV = 0.143, as for the unconfined concrete case) with the mean of 0.8%. It is noteworthy that the RV parameters $\varepsilon^c_{u,c}$ and $\varepsilon_{u,s}$ incorporated in this study shown to be important, but they are usually not considered explicitly in the numerical models in the literature. The sensitivity analysis shows that $\varepsilon_{u,s}$, the correlated RVs E_c, f_c and f_y induce the highest

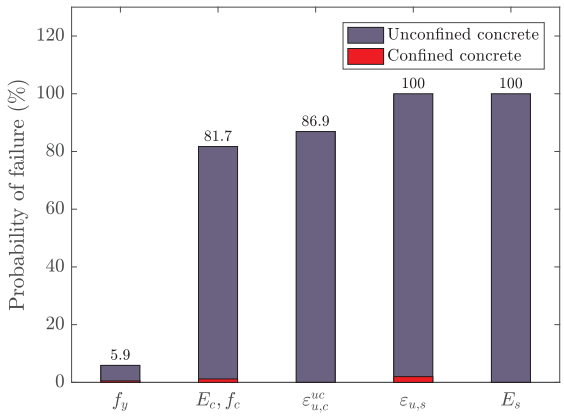

Fig. 8. Probability of failure for unconfined and confined concrete frames approximated from 1000 samples for each RV.

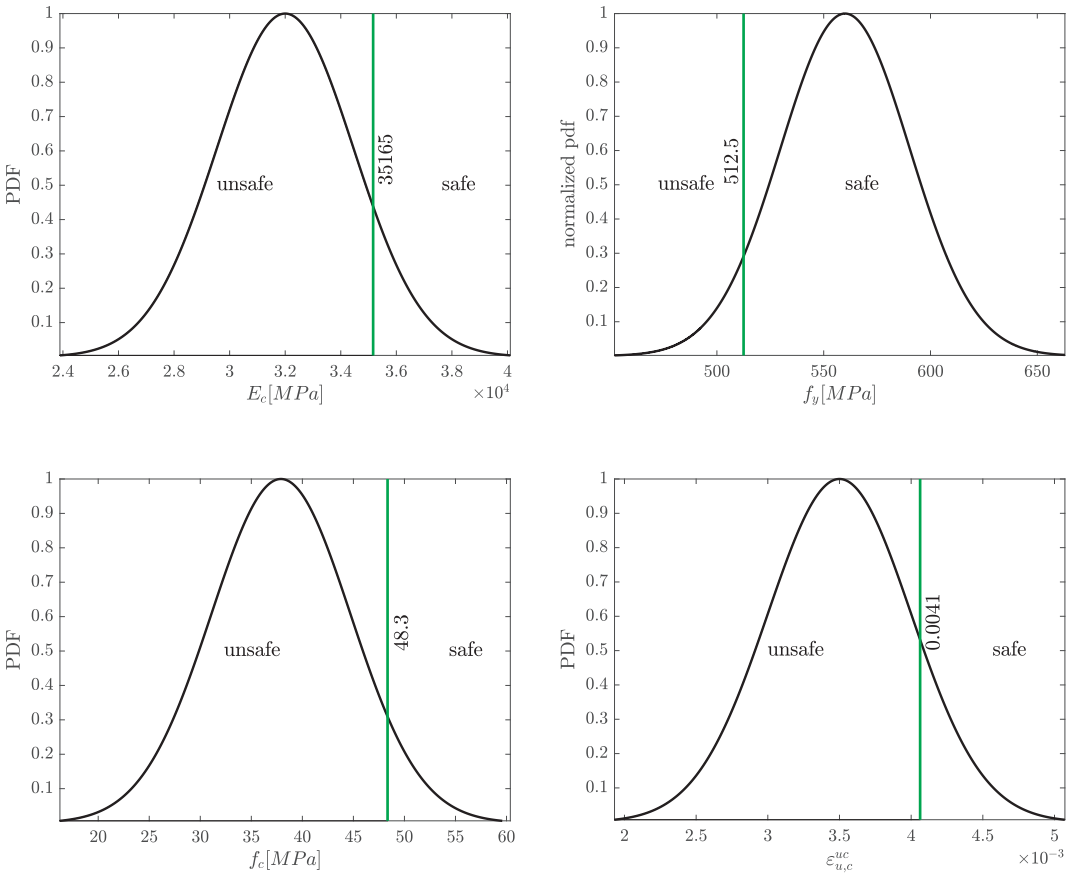

Fig. 9. Safe and unsafe domain (i.e. resulting in survival or collapse, respectively) of RVs considered separately for the unconfined concrete case (Fig. 6).

probability of failure for the confined concrete case, compared to other material parameters such as $\varepsilon^c_{u,c}$ and E_s. In order to *quantify accurately* the probabilities of failure of the confined concrete cases a significantly larger number of simulations would be required. Considering that such quantification *is not* the main focus of this contribution, this was not attempted in this work.

4.2.2. Residual displacement analysis for survived frames

This section investigates the residual vertical displacement at point C (v^c) of each survived frame, and its variability as a function of the considered RV. A higher residual displacement (i.e. structural deformation) indicates more intense irreversible events taking place after column loss. Fig. 10a and b show the maximum (v^c_{max}) and minimum (v^c_{min}) vertical displacements for each set of 1000

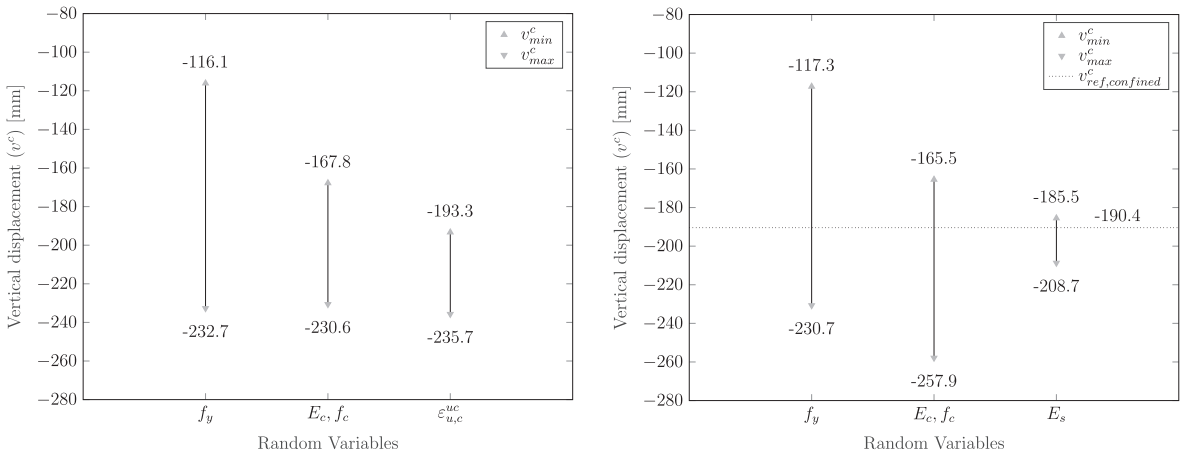

Fig. 10. Maximum, minimum and reference model residual vertical displacements for each survived frame for RV in the case of unconfined and confined concrete.

simulations for a given RV measured at 2 s after column loss.

The RVs f_y and correlated E_c, f_c variables present the highest discrepancy in both concrete cases. This can be explained by the fact that survived frames are in the catenary regime at the end of the analysis in which the influence of the steel reinforcement (in tension in the bay above the removed column) and concrete in compression near the connections is naturally larger. These variables critically influence the development of Compressive Arch Action (CAA) and Catenary Action (CA) that play an important role in the load transfer mechanism at the structural level after column loss. During the CAA E_c and f_c control the compressive concrete cracking, whereas f_y determines the tensile reinforcement yielding [11] in the catenary regime. Consequently, the results show that lower f_y values give a larger residual displacement (due to more plastic deformation of the reinforcement), while higher values present smaller residual displacements. The RVs E_s, $\varepsilon^c_{u,c}$ and $\varepsilon_{u,s}$ have limited influence on the residual vertical displacement, since E_s influences only the reinforcement elastic response and the residual displacement is mainly due to plastic straining (rebar fracture is limited). The influence of concrete ultimate strain ($\varepsilon_{u,c}$) is naturally larger in the unconfined concrete case. This can be explained by more intensive concrete crushing failure observed in the unconfined concrete cases and its sensitivity to $\varepsilon_{u,c}$. As expected, $\varepsilon^c_{u,c}$ and $\varepsilon_{u,s}$, have a small influence on the residual vertical displacement of the structure, because they are responsible for the concrete crushing and reinforcement breaking (respectively) that took place in the earlier stages of the analysis that ultimately led to survived structures, limiting their initial range to this scenario. It is noteworthy that, the confined concrete allows for the largest survive displacement as expected as a result of the higher ductility. Because of the insignificant variation of the residual vertical displacement for RVs $\varepsilon_{u,s}$ and $\varepsilon^c_{u,c}$ in the confined concrete case, these variables are not represented in Fig. 10b. This is of importance for future investigations where the number of RVs could be limited to a more reduced set.

As a summary of the sensitivity study, the results show that: (i) the performance of the RC structure to resist PC is critically influenced by concrete ductility; (ii) additionally E_c, f_c and f_y were also observed to have a relatively large influence on the structural robustness; (iii) $\varepsilon_{u,s}$ and $\varepsilon^c_{u,c}$ are found to be parameters with low influence on the residual displacement of survived frames and with a limited impact to resistance to collapse in the considered range; (iv) f_y presents the largest variability in the residual vertical displacement of survived frames due to the catenary action present in the survived structures supported by the reinforcement in tension.

5. RC frame probabilistic robustness assessment

In this section, the simultaneous variability of all six material properties is incorporated (as given in Table 1 and 2) to assess the structural response, damage evolution and mechanisms of failure in the SCL scenario of the RC frame studied in Section 4. Fig. 11a and b show the structural response as vertical displacement of point C vs. time curves for unconfined and confined concrete cases, respectively. Each figure contains the results of 1000 structural simulations with different random material parameter sets.

In *qualitative agreement* with the results of the sensitivity analysis (Section 4.2), the unconfined concrete case has a higher probability of failure than the confined concrete case, the trend is thus confirmed. An interesting result is that more unconfined concrete cases survived when all the RVs were varied simultaneously compared to Section 4. This is due to the nonlinear coupling of the material parameters effect on the structural response. While the current number of samples is *insufficient for quantifying* the probability of failure, it allows shedding light onto global tends in the structural behavior and failure/survival mechanisms.

5.1. Mechanisms of failure and PC resistance

This section presents the identified mechanisms of structural failure or resistance that led to the collapse or to survival of sudden

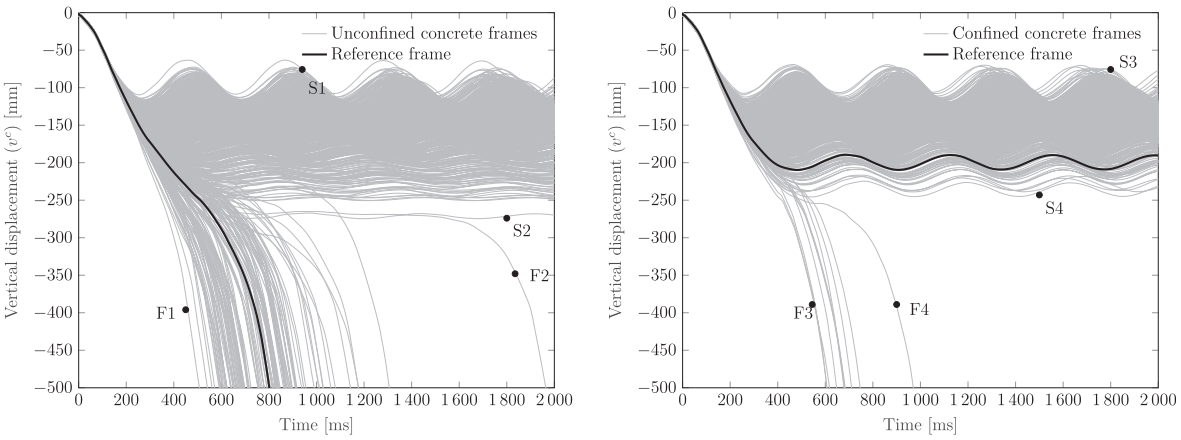

(a) Unconfined concrete model (b) Confined concrete model

Fig. 11. Vertical displacement of point C (v^c) vs. time curves from progressive collapse analysis of unconfined and confined concrete cases with all RV convoluted. Each figure shows the results of 1000 simulations.

column loss scenario. For this purpose some interesting survived and collapsed frame responses are chosen, as highlighted in Fig. 11 (S1, S2, S3, S4, F1, F2, F3 and F4), and the material parameter sets corresponding to each simulation are given in Table 4. The used multilayered framework has the capability to analyse at each time increment the structural and cross sectional states. The specific states of interest of the cross section considered here are: (i) reinforcement yielding; (ii) concrete crushing (iii) and reinforcement breaking. For clarity and simplicity, symbols are used in the figures to describe the structural degradation state, as summarized in Table 5.

The results show that the damage of the frame is restrained to the external bay initially supported by the removed column in all simulations. Internal force redistribution resulting in irreversible deformation and failure happens in this bay (similar to [16,50,17]), spreading gradually between the floors. As observed in experimental and numerical works [53–56], this study also confirms that the beam-column connections are the most critical elements, because failure always took place in such connections.

For the survived *unconfined concrete cases* S1 and S2 were chosen for the detailed analysis. Their structural state is shown in Fig. 12a and b at specific times after column loss. Frame S1 has the lowest residual vertical displacement at point C. This frame exhibits only the yielding of the reinforcements (Fig. 12a). The survival of this frame is due to the high strength of concrete and high steel yield strength. No concrete crushing is observed because of high values of E_c, f_c (Table 4) and despite of the low value of $\varepsilon_{u,s}$, the frame does not exhibit steel fracture because the high f_y delays steel yielding. The positive effect of the high value of these dominant material parameters matches the findings in Section 4.2. The cross section stress distribution of frame S1 is depicted on Fig. 13 for cross section A highlighted in Fig. 12a. The top concrete layers remain elastic and the bottom tensile reinforcement yields. The top steel rebars initially designed for compression start working in traction because of catenary action initiation.

Secondly, the survived frame S2 with largest residual vertical displacement at point C is analyzed. It is important to note that simulation S2 could be looked upon as a limit case for survival branching from the structural failure case F2 in Fig. 11a. The damage of this frame is characterized by: (i) the yielding of the reinforcements; (ii) crushing of concrete (in more than 30% of the cross sectional area) followed by (iii) axial strains in a layers reaching values close to the ultimate strain of steel right above the top tensile reinforcement. The structural failure mechanism or PC resistance spreads gradually from the bottom to the top floor. The difference in the structural behavior of cases S1 and S2 is explained by the lower concrete material parameters and lower steel yield strength for S2. Lower E_c, f_c (i.e. $E_c^{S2} = 0.73E_c^{S1}$ and $f_c^{S2} = 0.41f_c^{S1}$), explain the occurrence of concrete crushing in the S2 frame despite the high value of $\varepsilon_{u,c}^{uc,S2}$, as expected from the results in Section 4.2. The lower value of f_y^{S2} ($f_y^{S2} = 0.83f_y^{S1}$) allows an earlier yielding of the reinforcements, reaching earlier higher strain levels.

Table 4
Material parameters of structural simulations highlighted in Fig. 11, E_s is given for the sake of completeness, its influence was recognized to be negligible (Section 4.2).

Cases	Unconfined concrete				Confined concrete			
Frames	S1	S2	F1	F2	S3	S4	F3	F4
E_c (*GPa*)	34.90	25.35	28.74	28.60	40.10	23.89	33.95	24.69
f_c (*MPa*)	47.10	19.46	36.94	26.95	58.82	22.69	42.02	18.4
$\varepsilon_{u,c}$ (%)	0.36	0.40	0.18	0.31	0.87	0.76	0.75	0.75
E_s (*GPa*)	208.74	198.02	203.67	198.82	210.01	198.45	195.5	205.30
f_y (*MPa*)	659.41	549.01	513.56	546.88	610.5	520	460.58	513.70
$\varepsilon_{u,s}$ (%)	3.61	4.55	3.62	4.41	3.70	4.45	3.69	3.88

Table 5
Interpretation of the structural failure symbols used in Figs. 12,16 and 18.

Symbol	Interpretation
●	Yielding of the steel reinforcement
×	Failure of the steel reinforcement
△	Crushing of concrete in more than 30% of the section
▽	Crushing of concrete in less than 30% of the section

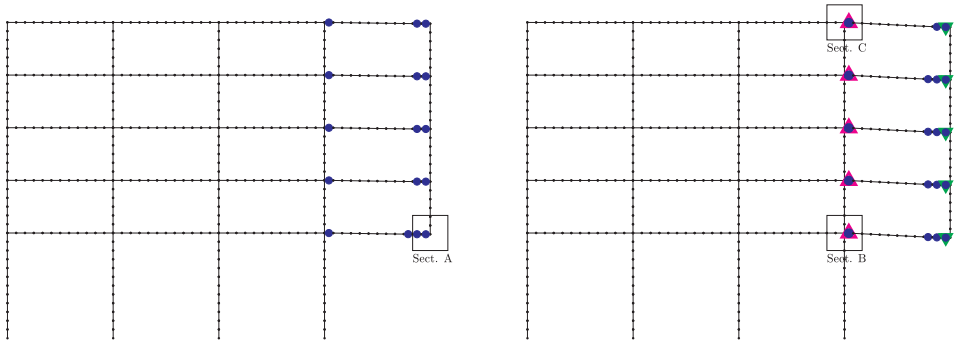

(a) Frame S1 stage at 940 ms (b) Frame S2 stage at 1500ms

Fig. 12. Structural damage mechanisms in survived frames of unconfined concrete cases.

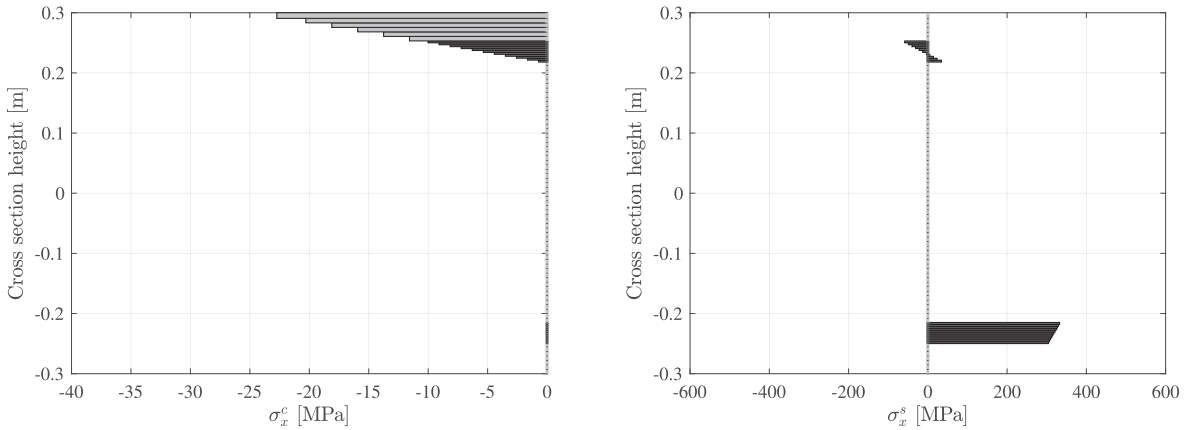

(a) S1 Concrete stress at 940 ms (b) S1 Steel stress at 940 ms

Fig. 13. Concrete and steel axial stress distribution in cross section A (Fig. 12a) with elastic concrete layers shown in grey and tensile reinforcement yielding shown in black.

The structural behavior is explained by considering the stress and layer state evolutions of cross section B (Fig. 14) and C (Fig. 15) highlighted in Fig. 12b. In cross section B, the ultimate strain of steel is surpassed in the layers right above the top rebar, with more than 30% of concrete layers crushed at 1500 ms after column loss. This can be considered as a limit case of structural survival, because already slightly higher generalized strains could lead to steel layer fracture initiation at the top of the rebars. In case of rebar breaking a gradual layer-by-layer steel failure can be observed, inherent to the computational model; actually the first rebar layer failure could indicate a full rebar fracture in a real life scenario.

The axial stress evolution at 0 ms (i.e. intact structure), 250 and 1500 ms after column loss for cross section C is given in Fig. 15. The stress levels in the design configuration under regular loads of the intact frame S2 (i.e. t = 0 ms) are in the elastic regime, as expected (Fig. 15a and b). After the column is removed (t = 250 ms), the bottom concrete cover and a few core layers of the concrete core fail by crushing (shown in green). Meanwhile, the top and bottom steel reinforcements are working in the plastic regime. At this stage high stress levels of axial stress for concrete and steel (i.e. $\sigma^c_{x,250ms} \approx 4 \times \sigma^c_{x,0ms}$ and $\sigma^s_{x,250ms} \approx 4.8 \times \sigma^s_{x,0ms}$) are developed. Concrete crushing is mainly due to CAA which diminishes with increasing concrete crushing and structural displacements. Eventually it gives place to the catenary action: at t = 1500 ms, the steel reinforcement layers start to transit from compression to tension at a

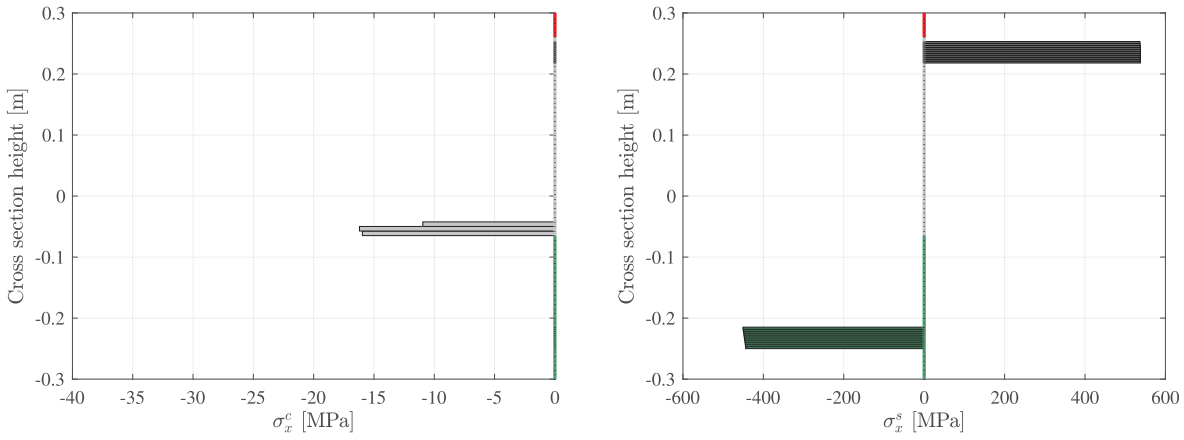

(a) S2 Concrete stress at 1500 ms (b) S2 Steel stress at 1500 ms

Fig. 14. Concrete and steel axial stress evolution in cross section B in (Fig. 12) with crushed concrete layers shown in green, tensile reinforcement yielding shown in black, axial strains larger than steel ultimate strain in red. (For interpretation of the references to colour in this figure legend, the reader is referred to the web version of this article.)

large residual displacement ($v^c \approx 275mm$).

The collapsed frames, F1 and F2 depicted in Fig. 16, both experienced the following failure mechanism (i) the yielding of the reinforcements; (ii) subsequent intense crushing of concrete accompanied by (iii) significant plastic deformation of the rebars in traction, similar to the survived frame S2, but with a catastrophic outcome of rebar breaking inducing structural failure. Comparing the material parameters between S2 (survival limit case branching off F2) and F2 it is apparent that the weaker concrete ($E_c^{S2} = 0.89E_c^{F2}$ and $f_c^{S2} = 0.72f_c^{F2}$) with similar ductility (i.e. $\varepsilon_{u,c}^{uc,S2} \approx \varepsilon_{u,c}^{uc,F2}$) is responsible for the larger extent of concrete crushing. This together with a similar yield strength of steel ($f_y^{F2} \approx f_y^{S2}$) with a lower ultimate strain ($\varepsilon_{u,s}^{F2} < \varepsilon_{u,s}^{S2}$) resulted in the structural collapse.

An important observation between the damage mechanism of survived (S1, S2) and collapsed (F1, F2) frames is that the concrete crushing happens much earlier, with higher intensity in collapsed frames due to lower values of $\varepsilon_{u,c}^{uc}$, i.e. $\varepsilon_{u,c}^{uc,F1} < \varepsilon_{u,c}^{uc,F2} < \varepsilon_{u,c}^{uc,S1} < \varepsilon_{u,c}^{uc,S2}$. The detrimental effect of concrete crushing on the structural behavior can be explained by the fact that it leads to a stress redistribution in the cross section resulting in higher stresses (and strains) in the steel rebars, ultimately leading to their fracture. In the present set of simulations with the adopted realistic range of steel material parameters it was observed that rebar fracture is an unavoidable consequence of concrete crushing beyond a critical extent in the cross section. Concrete crushing itself is highly dependent on $\varepsilon_{u,c}$, since it is determined by comparing total layer strain to the ultimate strain, but also E_c and f_c through the elasto-plastic strain history.

F1 presents the fastest collapse due to the lowest $\varepsilon_{u,c}^{uc,F1}$ and the relatively low value of f_y ($f_y^{S1} > f_y^{S2} > f_y^{F2} > f_y^{F1}$). As illustrated in Fig. 17 for cross sections D and E located at the same structural position in frames F1 and F2, respectively, F1 has more concrete layers crushed (in more than 30% of the cross sectional area) than F2 already at t = 300 ms (Fig. 17a and b). At t = 500 ms, F1 already failed by top and bottom reinforcements fracture (show in red), while a steel layers in cross section D already yielded and a few bottom rebars layers start to transit from compression to traction, followed later by the same top and bottom reinforcement fracture around 1750 ms (Fig. 11a). This delay in failure time is explained by the fact that F2 presents higher values of f_y and $\varepsilon_{u,s}$, than F1, allowing for internal forces redistributions and plastic energy dissipation in a larger time.

When considering *confined concrete cases*, the structural survival case S3 (Fig. 11) is very similar to S1, characterized by the reinforcement yielding only. This is explained by the strong concrete and high strength steel of frame S3, with $\varepsilon_{u,s}^{S1} \approx \varepsilon_{u,s}^{S3}$. It is interesting that frame S4 with the highest residual displacement among the confined concrete survived frames experienced (analogue to case S2 in the unconfined concrete simulations) only reinforcement yielding with low concrete crushing (less than 30% of the cross sectional area) without rebar fracture, in spite of the approximatively concrete and lower steel material parameters $E_c^{S4} \approx E_c^{S2}$; $f_c^{S4} \approx f_c^{S2}$ and $f_y^{S4} < f_y^{S2}$. This is due to the high value of the concrete and steel ultimate strains ($\varepsilon_{u,c}^{c,S4} = 1.9\varepsilon_{u,c}^{c,S2}$ and $\varepsilon_{u,s}^{S4} \approx \varepsilon_{u,s}^{S3}$), that impeded collapse and allowed for large plastic straining and energy dissipation. Due to the high values of $\varepsilon_{u,c}^{c}$ for confined cases, concrete crushing spreading in the cross section is limited and therefore is not a failure inducing phenomena, as opposed to the unconfined concrete cases. Fig. 19 illustrates the concrete and steel axial stress evolution in cross section F highlighted in (Fig. 18) with a few plastic layers in the concrete core and one concrete cover layer crushed. The structural failure for confined concrete cases is mainly governed by the rebar behavior because of very limited concrete crushing.

The collapsed frame F3 displayed in Fig. 18 exhibits the following failure sequence: (i) yielding of reinforcements and (ii) the fracture of reinforcements. No concrete crushing is observed which is different from the failure mechanism exhibited by unconfined concrete frames. Frame F3, despite of a relatively strong concrete ($E_c^{F3} = 1.42E_c^{S4}$ and $f_c^{F3} = 1.85f_c^{S4}$), presents low values of f_y and $\varepsilon_{u,s}$ (i.e $f_y^{F3} = 0.89f_y^{S4}$ and $\varepsilon_{u,s}^{F3} = 0.83\varepsilon_{u,s}^{S4}$) which explains the structural collapse by rebar fracture. The frame F4 exhibits the same mechanism of failure as F3 ending with catastrophic and abrupt rebars fracture. F3 is the quicker collapse case compared to F4 because

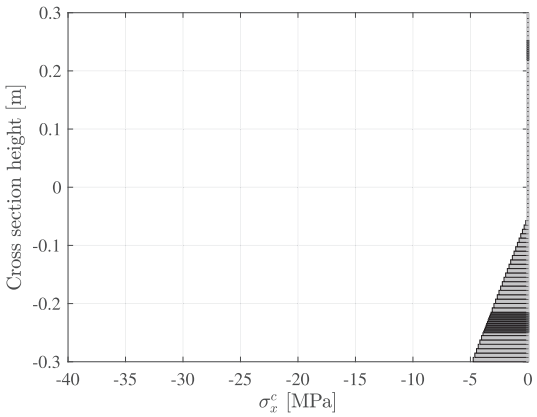

(a) S2 Design config. concrete (t = 0 ms)

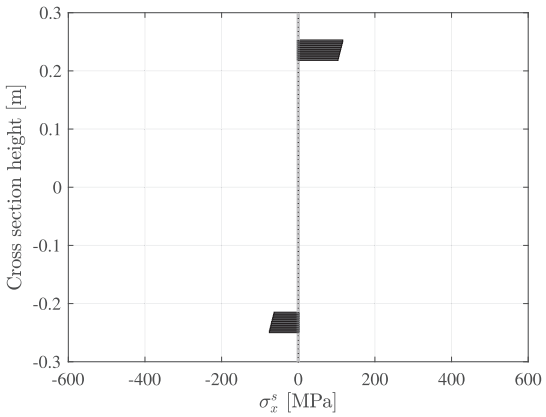

(b) S2 Design config. steel (t = 0 ms)

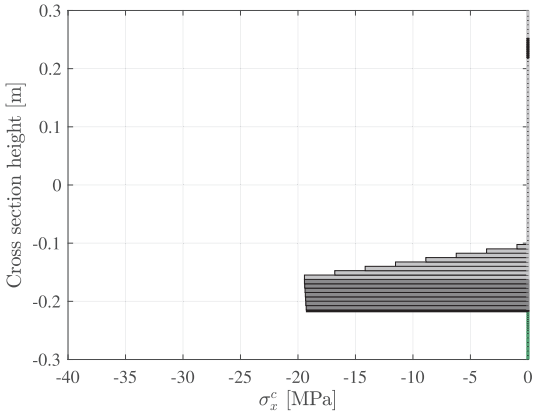

(c) S2 Concrete at t = 250 ms

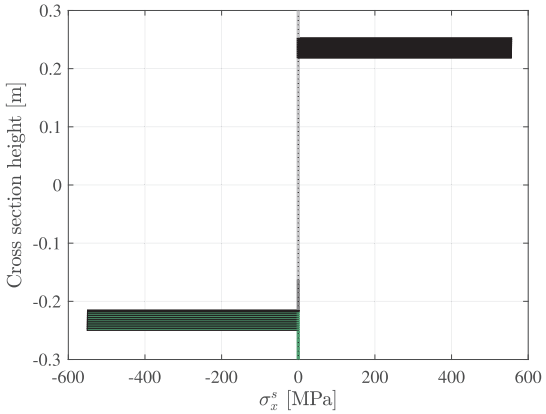

(d) S2 Steel at = 250 ms

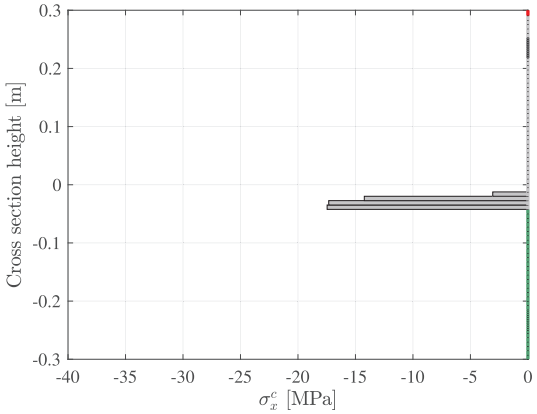

(e) S2 Concrete at t = 1500 ms

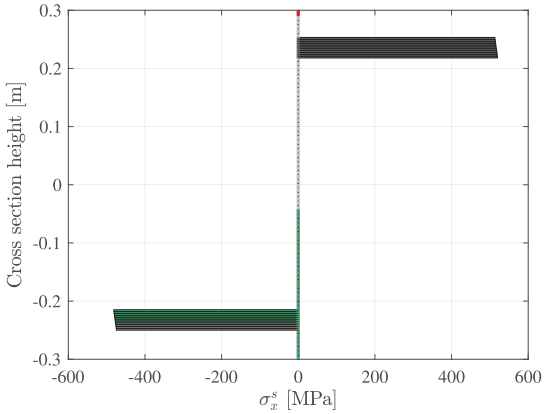

(f) S2 Steel at t = 1500 ms

Fig. 15. Concrete and steel axial stress evolution at cross section C in (Fig. 12) with plastic and crushed concrete layers shown in black and green, the tensile reinforcement yielding shown in black. (For interpretation of the references to colour in this figure legend, the reader is referred to the web version of this article.)

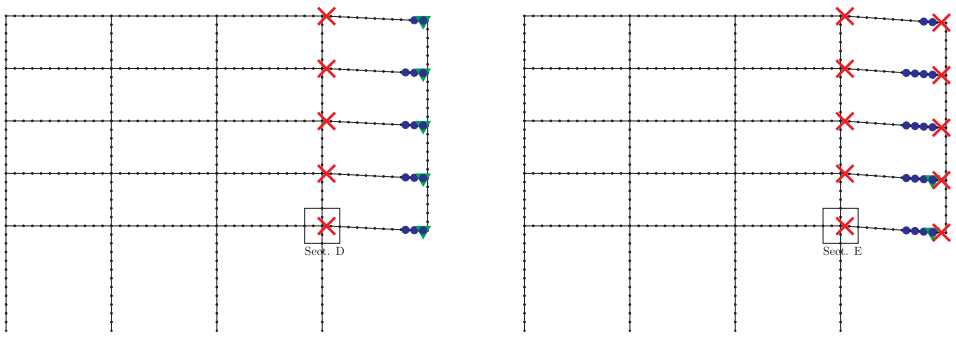

(a) Frame F2 stage at 1250 ms (b) Frame F1 stage at 460 ms

Fig. 16. Structural damage mechanisms in collapsed frames of unconfined concrete frame.

of the low values of steel yield strength ($f_y^{F3} < f_y^{F4}$) and ultimate strain in steel ($\varepsilon_{u,s}^{F3} < \varepsilon_{u,s}^{F4}$). Regarding the material parameters between S4 (survived case) and F4 (collapsed case) it is apparent that because of the similar values of the concrete parameters ($E_c^{F4} \approx E_c^{S4}$, $f_c^{F4} = 0.81 f_c^{S4}$ and $\varepsilon_{u,c}^{c,F4} \approx \varepsilon_{u,c}^{c,S4}$) the collapsed of F4 can be explained by the low value of f_y^{F4} and particularly the ultimate strain of steel ($\varepsilon_{u,s}^{F4} = 0.87 \varepsilon_{u,s}^{S4}$).

This observation is coherent with the reinforcement failure governed structural collapse of confined concrete cases, induced at high values of $\varepsilon_{u,c}$ observed in Section 4.

Providing sufficient ductility to concrete allows going from the *reinforcement yielding followed by intensive concrete crushing and subsequent rebar fracture* collapse chain to a *reinforcement yielding accompanied by a limited concrete crushing and subsequent rebar fracture* collapse chain, the latter being more controlled by the steel behavior (with a lower dispersion) and having a lower probability of collapse.

The numerical results were also post-processed in a performance-based philosophy, similar to [57,48]. Different limit states with increasing repair needs were defined, separated by damage ranges, as shown in Fig. 20. This choice is justified by a need to ensure on one the hand the sequential occurrence of limit states and increasing damage levels and on the other hand their suitability with the computational approach used in this study. In line with the literature [57,48] we distinguish between:

- *Immediate Occupancy (IO) limit state - Slight damage*: no considerable damage of the frame, the yielding of any of the constituents (concrete in compression, steel in compression or tension) is not observed, allowing immediate occupancy after slight structural repair (of concrete cracking in tension, taken into account by the zero-strength assumption of the used model).
- *Life safety (LS) - Moderate damage*: moderate concrete and steel yielding and moderate concrete cracking resulting in moderate repair in critical portions of the frame, considerable reduction in structural stiffness, the structure cannot be used before retro-fitting.
- *Collapse prevention (CP) - Extensive damage*: structural members damaged heavily, dramatic decrease in structural stiffness, large displacements, crushing of concrete and reinforcement yielding, the structure is close to collapse. Low safety for the occupants and need for major structural repair.
- *Progressive collapse*: partial or total collapse of the frame.

Taking benefit of the layered beam formulation offering local cross section state data, four damage zones linked to the above performance limit states were identified as follows:

- *Slight damage*: no yielding in concrete or steel; FE shown in black,
- *Moderate damage*: the yielding of any of the constituents is observed and less than 30% of concrete in the beam cross section is crushed; FE shown in green,
- *Extensive damage*: the yielding of any of the constituents is observed and more than 30% of the concrete cross section is crushed and/or bottom or top rebar fracture is observed; FE shown in orange,
- *Collapse*: both bottom and top rebars fracture; FE shown in red.

In order to assess structural damage employing the performance limit states defined below, the cross sectional data at each integration point of each finite element was studied at the end of the simulation, i.e. either at 2000 ms after column removal for frames that survive column loss or at the last increment for collapsed frames (Fig. 21). The findings of this assessment show that independently of the final outcome of the simulation, i.e. survival of column loss or collapse, the structural damage is systematically limited to the bay above the removed column, all members belonging to the other bays remain unaffected and therefore within the immediate occupancy limit state. This was observed for both unconfined and confined concrete cases. The structural collapse was also systematically limited to the bay above the removed column, because of elements near beam-column connections in the collapse limit state.

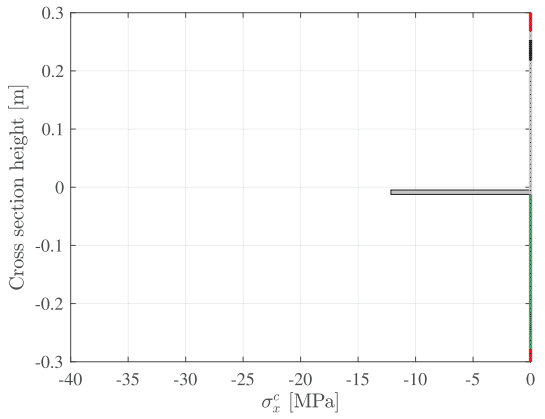

(a) F1 Concrete stress at 300 ms

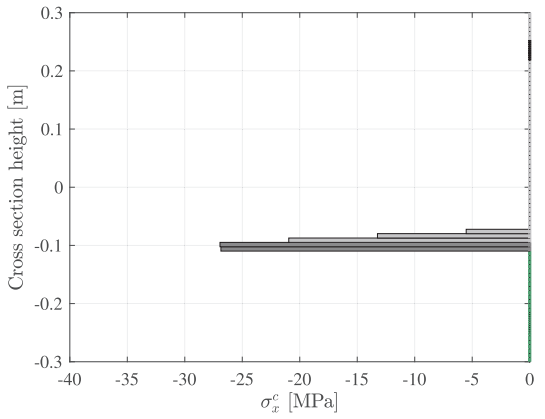

(b) F2 Concrete stress at 300 ms

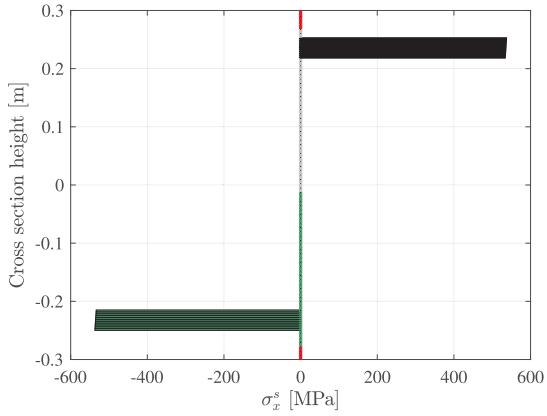

(c) F1 steel stress at 300 ms

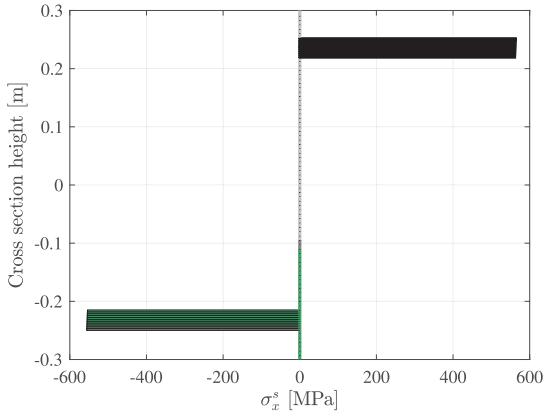

(d) F2 steel stress at 300 ms

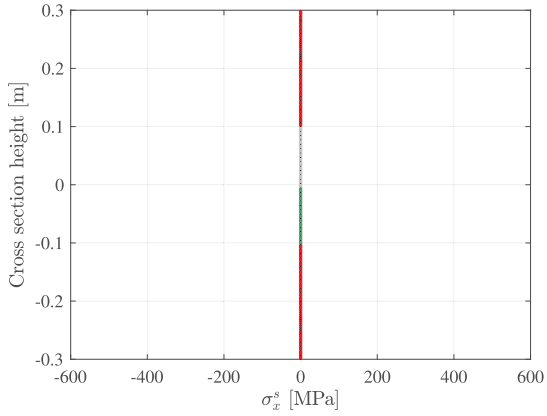

(e) F1 steel stress at 500 ms

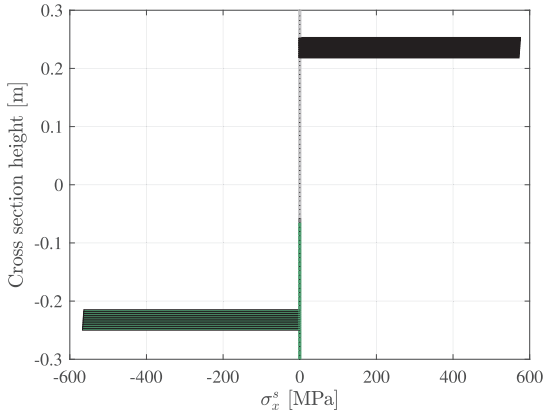

(f) F2 steel stress at 500 ms

Fig. 17. Concrete and steel axial stress evolution in cross sections D and E located in Fig. 16 with plastic and crushed concrete layers shown in black and green, the tensile reinforcement yielding shown in black and reinforcement failure in red. (For interpretation of the references to colour in this figure legend, the reader is referred to the web version of this article.)

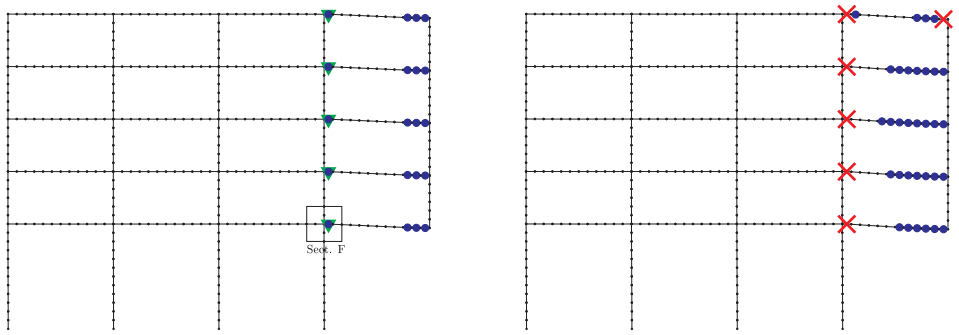

(a) Frame S4 stage at 1500ms (b) Frame F3 stage at 490ms

Fig. 18. Structural damage mechanisms in survived and collapsed frames of confined concrete cases.

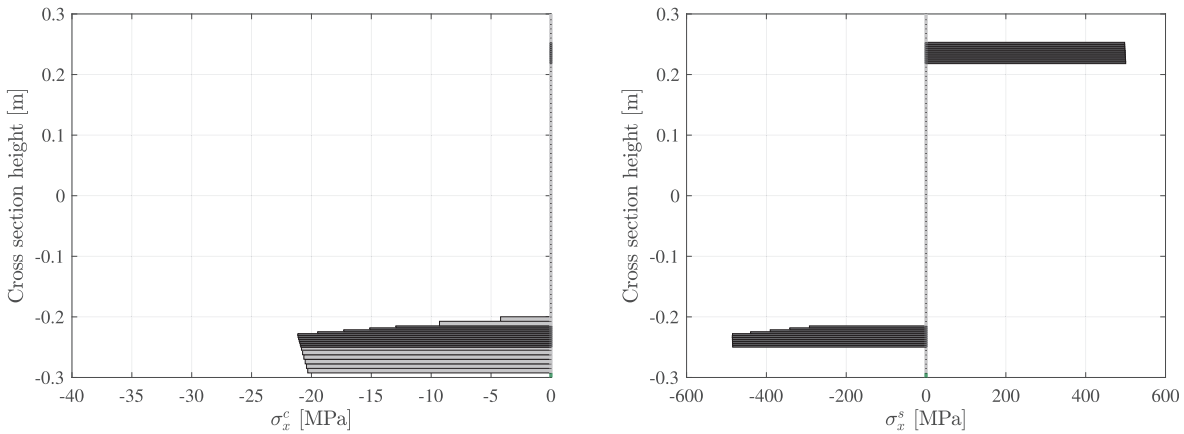

(a) S4 Concrete stress at 1500 ms (b) S4 Steel stress at 1500 ms

Fig. 19. Concrete and steel axial stress evolution in cross section F in (Fig. 18) with already plastic and crushed concrete layers shown in grey and green, the tensile reinforcement yielding shown in black. (For interpretation of the references to colour in this figure legend, the reader is referred to the web version of this article.)

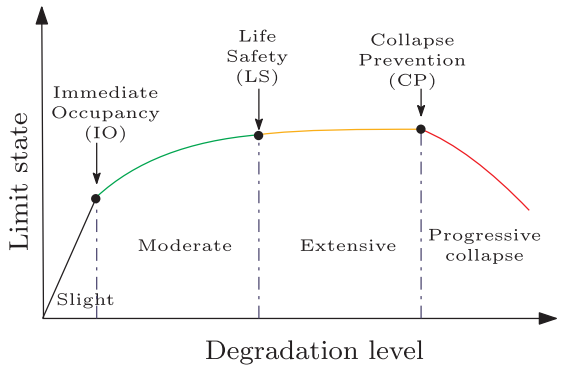

Fig. 20. Structural FE degradation and limits states based on [48,57].

For frames that survived the column removal the structural damage was observed to be proportional to the residual displacement, which is logical. The finite elements right next to the beam-column connexion of the bay above the removed column were in the moderate damage state for lower residual displacements while for the largest residual displacement these elements were in the extensive damage state. The bay above the removed column was in the life safety limit state for low residual displacements and entered the collapse prevention limit state for large residual displacements. Among the considered RV (E_c, f_c) showed the highest influence in terms of the number of damaged finite elements, followed by $\varepsilon_{u,c}^{uc}$ and f_y, which is in line with the conclusions drawn

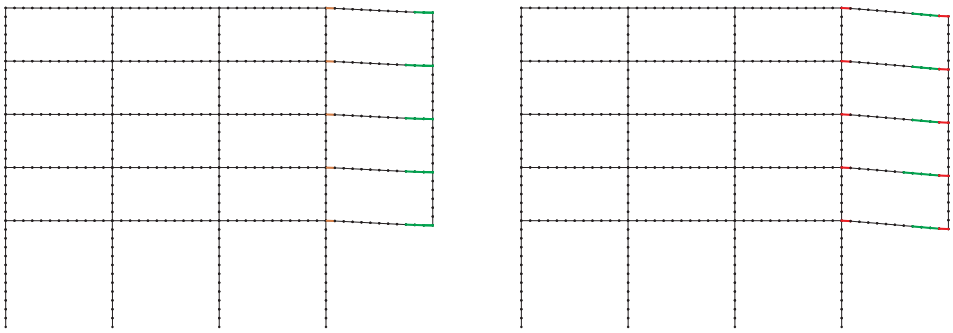

(a) Survived frame S2 (b) Collapsed frame F2

Fig. 21. Structural damage and limit state of extreme case F2 and S2 highlighted in Fig. 11 for unconfined concrete.

previously.

The results for survived and collapsed frames are very similar in terms of member damage states for both confined and unconfined concrete cases, i.e. (i) member damage is systematically limited to the bay above the removed column, (ii) collapse is induced by critical damage (collapse limit state) of the beams close to column-beam joints, (iii) the damage is proportional to the residual displacement for the frames that survive column loss, (iv) for survived frames the damage limit state never exceeds the extensive damage limit state, as expected.

The material parameters observed to be critical and their effects in this section are aligned with the findings of Section 4.2. If the load redistribution after column loss can happen (highly dependent on concrete ductility), it can lead to the appearance of beneficial catenary effects. At this stage concrete plays a smaller role (zero tensile strength assumption in this study) and mainly the reinforcement parameters $\varepsilon_{u,s}$ govern the ultimate failure of structure. Parameters f_y and $\varepsilon_{u,s}$ determine the ultimate rebar fracture, the last step in the chain of events leading to collapse for both confined and unconfined concrete cases.

6. Conclusions and outlook

In this study, the influence of material properties variability on RC structures capacity to mitigate PC was investigated using a LHS correlation reduction technique coupled with a 2D, in-house developed nonlinear dynamic multilayered beam framework. Six RVs of the material behavior of the constituents were identified and each RV was considered separately first in a sensitivity study. Secondly, the robustness of the RC frame was assessed varying all RV simultaneously.

In the light of the results, the following main conclusions are drawn:

1. taking into account realistic material parameter uncertainties in RC structures can lead to collapse or survival of the structure, with a large influence of $\varepsilon_{u,c}$, E_c, f_c, $\varepsilon_{u,s}$ and f_y;
2. the robustness of RC structures is significantly enhanced by increasing concrete ductility, represented phenomenologically in this work by varying $\varepsilon_{u,c}$ in physically sound ranges for unconfined and confined concrete cases;
3. f_y was observed to induce the largest variability in the residual displacement of frames surviving column loss, because of the natural influence of steel behavior in the final catenary regime;
4. in the studied cases structural damage did not spread beyond the bay adjacent to the removed column and beam-columns connections were confirmed to be the most critical elements concentrating irreversible phenomena;
5. different chains of events leading to collapse were identified for unconfined and confined concrete cases with a lower probability of failure for confined concrete;
6. the correct design of stirrups is crucial in order to ensure an appropriate ductility of concrete, especially in the areas close to column-beam joints, where the structural failure happens the most frequently; establishing a proper quantitative link between the stirrup design and the resulting ultimate strain of concrete is therefore identified as future work of high relevance.

Based on the findings, the following set of practical recommendations for enhanced structural robustness to PC can be formulated:

- the correct design of stirrups is crucial in order to ensure an appropriate ductility of concrete, especially close to structural joints, where the structural failure happens the most frequently;
- the quality of the steel reinforcements, especially their yield strength and ultimate strain have to be closely controlled, since these parameters were observed to have a large influence on the plastic events after the column loss and on the residual displacements of structures that resist to this scenario;
- in order for a structure to survive column loss it was observed that ensuring that the proper cross sectional history (survival mechanism) can be followed by providing appropriate material ductility of the constituents is crucial.

Further research of immediate interest is to investigate material variability effects on structures designed following different building codes, including strain-rate effects and the column removal time [16]. Lifting strain compatibility by incorporating bond slip [37] in the numerical model incorporating stirrups failure, the extension to 3D model and analysis of other ground floor column loss are possible future works.

Declaration of Competing Interest

The authors declare that they have no known competing financial interests or personal relationships that could have appeared to influence the work reported in this paper.

Acknowledgement

The second and third authors gratefully acknowledge the Coordenação de Aperfeiçoamento de Pessoal de Nível Superior, (CAPES) and the National Council for Scientific and Technological Development, CNPq of Brazil (Process number 140458/2017–4).

References

[1] European Committee for Standardization (CEN). Design of concrete structures-Part 1-1: General rules and rules for buildings. Eur. Comm. Stand. Brussels, 2004.
[2] Department of Defense (DoD). Unified facilities criteria: design of buildings to resist progressive collapse. Technical report, UFC 4-023-03. United States Department of Defense, 2009.
[3] General Services Administration (GSA). Progressive collapse analysis and design guidelines for new federal office buildings and major modernization projects. Technical report, Washington, DC, United States, 2003.
[4] UFC 4-023-03. Design of buildings to resist progressive collapse. Technical report, US Army Corps of Engineering Washington DC, USA, 2010.
[5] B.R. Ellingwood, R. Smilowitz, D.O. Dusenberry, D. Duthinh, H.S. Lew, N.J Carino, Best practices for reducing the potential for progressive collapse in buildings. U.S, Natl. Inst. Stand. Technol. (NIST) (2007).
[6] X.H. Yu, D.G. Lu, K. Qian, B. Li, Uncertainty and sensitivity analysis of reinforced concrete frame structures subjected to column loss, J. Perform. Constr. Facili. 31 (1) (2016) 04016069.
[7] J. Park, J. Kim, Fragility analysis of steel moment frames with various seismic connections subjected to sudden loss of a column, Eng. Struct. 32 (6) (2010) 1547–1555.
[8] J. Kim, J.H. Park, T.H. Lee, Sensitivity analysis of steel buildings subjected to column loss, Eng. Struct. 33 (2) (2011) 421–432.
[9] G. Xu, B.R. Ellingwood, Probabilistic robustness assessment of pre-northridge steel moment resisting frames, J. Struct. Eng. 137 (9) (2011) 925–934.
[10] J.L. Le, B. Xue, Probabilistic analysis of reinforced concrete frame structures against progressive collapse, Eng. Struct. 76 (2014) 313–323.
[11] D.C. Feng, S.C. Xie, W.N. Deng, Z.D. Ding, Probabilistic failure analysis of reinforced concrete beam-column sub-assemblage under column removal scenario, Eng. Fail. Anal. 100 (2019) 381–392.
[12] S. Szyniszewski, Effects of random imperfections on progressive collapse propagation, Struct. Congr. 2010 (2010) 3572–3577.
[13] M.H. Tsai, B.H. Lin, Dynamic amplification factor for progressive collapse resistance analysis of an rc building, Struct. Des. Tall Special Build. 18 (5) (2009) 539–557.
[14] E. Brunesi, R. Nascimbene, Extreme response of reinforced concrete buildings through fiber force-based finite element analysis, Eng. Struct. 69 (2014) 206–215.
[15] A. Fascetti, S.K. Kunnath, N. Nisticò, Robustness evaluation of rc frame buildings to progressive collapse, Eng. Struct. 86 (2015) 242–249.
[16] B. Iribarren, P. Berke, Ph. Bouillard, J. Vantomme, T.J. Massart, Investigation of the influence of design and material parameters in the progressive collapse analysis of RC structures, Eng. Struct. 33 (2011) 2805–2820.
[17] K. Menchel, T.J. Massart, Y. Rammer, Ph. Bouillard, Comparison and study of different progressive collapse simulation techniques for RC structures, J. Struct. Eng. 135 (6) (2009) 685–697.
[18] C.E.M. Oliveira, E.A.P. Batelo, P.Z. Berke, R.A.M. Silveira, T.J. Massart, Nonlinear analysis of the progressive collapse of reinforced concrete plane frames using a multilayered beam formulation, IBRACON Struct. Mater. J. 7 (2014) 845–855.
[19] E. Brunesi, R. Nascimbene, F. Parisi, N. Augenti, Progressive collapse fragility of reinforced concrete framed structures through incremental dynamic analysis, Eng. Struct. 104 (2015) 65–79.
[20] European Committee for Standardization (CEN). Design of structures for earthquake resistance-Part 1.5: Specific rules for concrete buildings. Eur. Comm. Stand. Brussels, 2004.
[21] A.H. Arshian, G. Morgenthal, Probabilistic assessment of the ultimate load-bearing capacity in laterally restrained two-way reinforced concrete slabs, Eng. Struct. 150 (2017) 52–63.
[22] H.M. Elsanadedy, Y.A. Al-Salloum, T.H. Almusallam, T. Ngo, H. Abbas, Assessment of progressive collapse potential of special moment resisting rc frames-experimental and fe study, Eng. Fail. Anal. (2019).
[23] S. Mazzoni, F. McKenna, M.H. Scott, G.L. Fenves, Computer program opensees: Open system for earthquake engineering simulation, Pacific Earthquake Engineering Research Center (PEER), University of California, Berkeley, California, 2009.
[24] Seimosoft Seimostruct. A computer program for static and dynamic nonlinear analysis of framed structures. URL: http://www. seismosoft. com, 2004.
[25] S. Amiri, H. Saffari, J. Mashhadi, Assessment of dynamic increase factor for progressive collapse analysis of rc structures, Eng. Fail. Anal. 84 (2018) 300–310.
[26] A. Olsson, G. Sandberg, O. Dahlblom, On latin hypercube sampling for structural reliability analysis, Struct. Saf. 25 (1) (2003) 47–68.
[27] A.M.J. Olsson, G. Sandberg, Latin hypercube sampling for stochastic finite element analysis, J. Eng. Mech. 128 (1) (2002) 121–125.
[28] T. Xu, T. Xiang, R. Zhao, G. Yang, C. Yang, Stochastic analysis on flexural behavior of reinforced concrete beams based on piecewise response surface scheme, Eng. Fail. Anal. 59 (2016) 211–222.
[29] A.H. Arshian, G. Morgenthal, S. Narayanan, Influence of modelling strategies on uncertainty propagation in the alternate path mechanism of reinforced concrete framed structures, Eng. Struct. 110 (2016) 36–47.
[30] P.Z. Berke, T.J. Massart, Modelling of stirrup confinement effects in RC layered beam finite elements using a 3D yield criterion and transversal equilibrium constraints, Int. J. Concr. Struct. Mater. 12 (2018) 49.
[31] R.S. Oliveira, M.A. Ramalho, M.R.S. Corrêa, A layered finite element for reinforced concrete beams with bond-slip effects, Cem. Concr. Compos. (2008).
[32] M.A. Crisfield, Non-linear Finite Element Analysis of Solids and Structures: Advanced Topics, vol. 2, John Wiley & Sons, 1997.
[33] Kai Qian, Bing Li, Experimental and analytical assessment on rc interior beam-column subassemblages for progressive collapse, J. Perform. Constr. Facil. 26 (5) (2012) 576–589.
[34] K. Qian, B. Li, Performance of three-dimensional reinforced concrete beam-column substructures under loss of a corner column scenario, J. Struct. Eng. 139 (4) (2012) 584–594.
[35] J. Yu, K.H. Tan, Experimental and numerical investigation on progressive collapse resistance of reinforced concrete beam column sub-assemblages, Eng. Struct. 55 (2013) 90–106.
[36] J. Hou, L. Song, Progressive collapse resistance of rc frames under a side column removal scenario: The mechanism explained, Int. J. Concr. Struct. Mater. 10 (2)

(2016) 237–247.
[37] R.S. Oliveira, M.A. Ramalho, M.R.S. Corrêa, A layered finite element for reinforced concrete beams with bond–slip effects, Cem. Concr. Compos. 30 (3) (2008) 245–252.
[38] S.A. Mirza, J.G. MacGregor, M. Hatzinikolas, Statistical descriptions of strength of concrete, J. Struct. Divis. 105 (6) (1979) 1021–1037.
[39] B. Ellingwood, Development of a Probability Based Load Criterion for American National Standard A58: Building Code Requirements for Minimum Design Loads in Buildings and Other Structures, vol. 13, US Department of Commerce, National Bureau of Standards, 1980.
[40] C.G. Trezos, Reliability considerations on the confinement of rc columns for ductility, Soil Dynam. Earthq. Eng. 16 (1) (1997) 1–8.
[41] S.A. Mirza, J.G. MacGregor, Variability of mechanical properties of reinforcing bars, J. Struct. Div., 105(ASCE 14590 Proceeding), 1979.
[42] JCSS. Probabilistic model code. Joint Committee on Structural Safety, 2001.
[43] B. Xue, J.L. Le, Stochastic computational model for progressive collapse of reinforced concrete buildings, J. Struct. Eng. 142 (7) (2016) 04016031.
[44] E. Brunesi, F. Parisi, Progressive collapse fragility models of european reinforced concrete framed buildings based on pushdown analysis, Eng. Struct. 152 (2017) 579–596.
[45] D. Celarec, M. Dolšek, The impact of modelling uncertainties on the seismic performance assessment of reinforced concrete frame buildings, Eng. Struct. 52 (2013) 340–354.
[46] B. Xue, J.L. Le, Simplified energy-based analysis of collapse risk of reinforced concrete buildings, Struct. Saf. 63 (2016) 47–58.
[47] T.H. Lee, K.M. Mosalam, Probabilistic fiber element modeling of reinforced concrete structures, Comput. Struct. 82 (27) (2004) 2285–2299.
[48] F. Parisi, M. Scalvenzi, E. Brunesi, Performance limit states for progressive collapse analysis of reinforced concrete framed buildings, Struct. Concr. 20 (1) (2019) 68–84.
[49] Diamonds2010. r.01. buildsoft, http://www.buildsoft.eu, 2010.
[50] M.H. Tsai, B.H. Lin, Investigation of progressive collapse resistance and inelastic response for an earthquake-resistant rc building subjected to column failure, Eng. Struct. 30 (12) (2008) 3619–3628.
[51] S. Kokot, A. Anthoine, P. Negro, G. Solomos, Static and dynamic analysis of a reinforced concrete flat slab frame building for progressive collapse, Eng. Struct. 40 (2012) 205–217.
[52] G.V. Gudmundsson, B.A. Izzuddin, The 'sudden column loss' idealisation for disproportionate collapse assessment, Struct. Eng. 88 (6) (2010) 22–26.
[53] J. Yu, K.H. Tan, Structural behavior of rc beam-column subassemblages under a middle column removal scenario, J. Struct. Eng. 139 (2) (2012) 233–250.
[54] H.S. Lew, Y. Bao, F. Sadek, J.A. Main, S. Pujol, M.A. Sozen, An experimental and computational study of reinforced concrete assemblies under a column removal scenario, NIST Technical Note 1720 (2011) 106.
[55] D. Gouverneur, R. Caspeele, L. Taerwe, Experimental investigation of the load–displacement behaviour under catenary action in a restrained reinforced concrete slab strip, Eng. Struct. 49 (2013) 1007–1016.
[56] S. Li, S. Shan, C. Zhai, L. Xie, Experimental and numerical study on progressive collapse process of rc frames with full-height infill walls, Eng. Fail. Anal. 59 (2016) 57–68.
[57] M.S.C Garcia, G.H Siqueira, L.C.M.V. Junior, I. Vizotto, Evaluation of structural capacity of triangular and hexagonal reinforced concrete free-form shells, Eng. Struct. 188 (2019) 519–537.